metals

MDPI

Article

Phase Equilibria Studies in the CaO-MgO-Al_2O_3-SiO_2 System with Al_2O_3/SiO_2 Weight Ratio of 0.4

Jinfa Liao [1], Gele Qing [2] and Baojun Zhao [1,3,*]

[1] International Institute for Innovation, Jiangxi University of Science and Technology, Nanchang 330013, China
[2] Shougang Research Institute of Technology, Beijing 100043, China
[3] Sustainable Minerals Institute, University of Queensland, Brisbane, QLD 4072, Australia
* Correspondence: bzhao@jxust.edu.cn

Abstract: With the raw materials for ironmaking becoming increasingly complex, more accurate phase equilibrium information on the slag is needed to refine the blast furnace operation to reduce the energy cost and CO_2 emissions. CaO-SiO_2-Al_2O_3-MgO is a basic system of ironmaking slag in which CaO and MgO mainly come from the flux, SiO_2 and Al_2O_3 are mainly from raw materials. The effect of flux additions on the phase equilibrium of the slag can be described by a pseudo-ternary system CaO-MgO-(Al_2O_3+SiO_2) at a fixed Al_2O_3/SiO_2 ratio of 0.4. Liquidus temperatures and solid solutions in the CaO-MgO-Al_2O_3-SiO_2 system with Al_2O_3/SiO_2 weight ratio of 0.4 have been experimentally determined using high temperature equilibration and quenching techniques followed by electron probe microanalysis. Dicalcium silicate (Ca_2SiO_4), cordierite ($2MgO{\cdot}2Al_2O_3{\cdot}5SiO_2$), spinel ($MgO{\cdot}Al_2O_3$), merwinite ($3CaO{\cdot}MgO{\cdot}2SiO_2$), anorthite ($CaO{\cdot}Al_2O_3{\cdot}2SiO_2$), mullite ($Al_2O_3{\cdot}SiO_2$), periclase (MgO), melilite ($2CaO{\cdot}MgO{\cdot}2SiO_2$-$2CaO{\cdot}Al_2O_3{\cdot}SiO_2$) and forsterite ($Mg_2SiO_4$) are the major primary phases in the composition range investigated. A series of pseudo-binary phase diagrams have been constructed to demonstrate the application of the phase diagrams on blast furnace operation. Composition of the solid solutions corresponding to the liquidus have been accurately measured and will be used for the development of the thermodynamic database.

Keywords: phase equilibria; liquidus temperature; CaO-MgO-Al_2O_3-SiO_2 system; blast furnace slag; basicity

check for updates

Citation: Liao, J.; Qing, G.; Zhao, B. Phase Equilibria Studies in the CaO-MgO-Al_2O_3-SiO_2 System with Al_2O_3/SiO_2 Weight Ratio of 0.4. *Metals* **2023**, *13*, 224. https://doi.org/10.3390/met13020224

Academic Editors: Fernando Castro and Mark E. Schlesinger

Received: 7 December 2022
Revised: 13 January 2023
Accepted: 19 January 2023
Published: 25 January 2023

Copyright: © 2023 by the authors. Licensee MDPI, Basel, Switzerland. This article is an open access article distributed under the terms and conditions of the Creative Commons Attribution (CC BY) license (https://creativecommons.org/licenses/by/4.0/).

1. Introduction

Due to the shortage of high-grade iron ore resources and the increasingly fierce competition in the steel market, many steel enterprises face the use of low-quality raw materials [1]. However, a variety of negative problems, including incomplete separation of slag and hot metal, difficult tapping of the slag from the blast furnace and inefficient reaction between slag and hot metal, can happen when using low-quality raw materials [2–4]. On the other hand, a modern blast furnace with automatic operating system can adjust the parameters accurately if the required information is available. Hence, more accurate slag phase equilibrium information should be provided for modern blast furnaces to treat complex raw materials [5–7]. The oxide system CaO-MgO-Al_2O_3-SiO_2 forms a base for ironmaking slags. SiO_2 and Al_2O_3 are mainly from raw materials such as iron ores, coke and coal. CaO and MgO are mainly added as flux to adjust the slag composition to obtain the required properties.

Phase equilibrium information of the CaO-MgO-Al_2O_3-SiO_2 system has been studied by many scholars [8–23]. Slag Atlas summarized the CaO-MgO-Al_2O_3-SiO_2 system based on the earlier studies [24]. The phase diagrams reported were presented in the form of CaO-MgO-SiO_2 pseudo-ternary sections at fixed Al_2O_3 concentrations [10] or Al_2O_3-CaO-SiO_2 pseudo-ternary sections at fixed MgO concentrations [11–13]. Due to the limitations of the experimental techniques, earlier studies [8–14] only determined the liquidus temperatures without the composition of the solid solutions. Significant differences were also observed

between the reported results [9,10,14]. With the development of the ironmaking techniques, previous phase diagrams are not enough to provide accurate operation guidelines. CaO/SiO_2 is usually fixed for a given blast furnace to obtain stable liquidus temperature of the slag and sulfur removal. Phase equilibria in the $(CaO+SiO_2)$-MgO-Al_2O_3 system have been investigated recently at fixed CaO/SiO_2 weight ratios of 0.9, 1.1, 1.3 and 1.5 [15–18]. With this information, MgO addition corresponding to the Al_2O_3 concentrations in the slag can be adjusted to maintain the stable liquidus temperatures. When a blast furnace has a stable supply of the raw materials, the Al_2O_3/SiO_2 weight ratio in the slag is relatively fixed. Addition of CaO and MgO in different ratios and amounts can confer different properties of the slag including liquidus temperature and sulfur capacity. The existing phase diagrams summarized above cannot provide the detailed phase equilibrium information for various CaO and MgO additions. In addition, powerful thermodynamic software such as FactSage [25] and Thermo-Calc [26] have been developed to predict liquidus temperatures of the slags. It was found that there are still differences between the experimental results and the predicted results, indicating that the thermodynamic database needs to be optimized. Experimentally determined liquidus temperatures and corresponding compositions of the solid solutions can provide accurate data to support the development of a reliable thermodynamic database.

In this study, the phase equilibria of the CaO-MgO-Al_2O_3-SiO_2 system at a fixed Al_2O_3/SiO_2 weight ratio of 0.4 were experimentally investigated using a high-temperature equilibration, quenching and electron probe microanalysis (EPMA) method. Effects of the flux ratio MgO/CaO and quaternary basicity $(CaO+MgO)/(Al_2O_3+SiO_2)$ on liquidus temperature will be discussed. The experimental results will be compared with FactSage predictions to evaluate the existing thermodynamic database.

2. Experimental

The experimental procedure includes sample preparation from pure chemicals, high-temperature equilibration, and analyses of the microstructures and compositions of the phases present in the quenched samples. The experiments were first planned based on the available information, including low-order phase diagrams, FactSage predictions and preliminary experiments. High purity powders of Al_2O_3, SiO_2, MgO and $CaCO_3$ were weighed and mixed according to the experimental plan and pelletized. An approximately 0.2 g pellet was placed in a graphite crucible (inner diameter 5 mm and height 5 mm). Equilibration experiments were carried out in a vertical tube furnace (recrystallized alumina as a reaction tube, 30 mm inner diameter). The graphite crucible, which contained the pelletized mixtures was suspended using a platinum wire (0.5 mm diameter). Argon gas (flow rate: 500 mL/min) was passed through the furnace during the experiment to avoid oxidization of the crucible. The sample was pre-melted at a temperature 20–50 °C higher than the equilibration temperature for 30 min. Then the temperature was lowered to the desired temperature and kept for a time sufficient to achieve equilibrium. The equilibration usually took from 2 to 12 h, depending on the viscosity of the slag, which is related to the composition and temperature. For example, a shorter time was employed at higher temperatures or with lower-silica slag. Several steps were taken to ensure the equilibrium was reached in the system. First, preliminary experiments were carried out for different periods at the beginning of the project. The sufficient time was determined by the same phase compositions obtained over the reaction period. The actual reaction time was always much longer than that from the preliminary experiments. Second, uniform microstructure and liquid composition from different areas of the quenched sample confirmed the equilibrium. Third, self-consistence of all experimental data was checked to confirm the equilibrium.

After equilibration, the sample was dropped into water directly to attain rapid cooling. The quenched samples were mounted in epoxy resin, polished and carbon-coated for electron probe microanalysis (EPMA). A JXA 8200 (Japan Electron Optics Ltd., Tokyo, Japan) Electron Probe Microanalyser with Wavelength Dispersive Spectroscopy (WDS,

Japan Electron Optics Ltd., Tokyo, Japan) was used for microstructural and compositional analyses. The EPMA was operated at an accelerating voltage of 15 kV and a probe current of 15 nA. The beam size was set to "0 μm" to accurately measure the composition of an area larger than 1 μm. The ZAF (Z is atomic number correction factor, A is absorption correction factor, and F is fluorescence correction factor) correction procedure was applied for the data analysis. The standards used for EPMA included alumina (Al_2O_3) for Al, magnesia (MgO) for Mg, and wollastonite ($CaSiO_3$) for Ca and Si. These standards were provided by Charles M Taylor Co., Stanford, CA, USA. The average accuracy of the EPMA measurements was within ±1 wt%.

On rapid cooling, the liquid phase in the equilibrated sample was converted to homogeneous glass and the solid phases were retained in their shapes and compositions. The homogeneity of the phases can be confirmed by the EPMA measurements in different areas of the quenched sample. Usually, 8–20 points of the liquid phase and 3–5 points of the solid phase were measured from different areas by EPMA. The samples with the standard deviation of the phase compositions less than 1% were accepted for phase diagram construction.

FactSage 8.2 [25] was used for the thermodynamic calculations that are compared with the experimental results. The databases of "FactPS" and "FToxid" were used in the "Equilib" module. The solution phases selected in the calculations were "FToxide-SLAGA", "FToxide-SPINC", "FToxide-MeO_A", "FToxide-bC2S", "FToxide-aC2S", "FToxide-Mel", "FToxide-WOLLA, "FToxide-OlivA" and "FToxide-Mull".

3. Results and Discussion

3.1. Description of the Pseudo-Ternary Section

Proper presentation of the multi-component phase diagram is essential for easy use by industrial operators and academic researchers. Figure 1 shows the presentation of the pseudo-ternary phase diagram CaO-MgO-(Al_2O_3+SiO_2) at a fixed Al_2O_3/SiO_2 weight ratio of 0.4. The end members of the pseudo-ternary section are CaO, MgO and (Al_2O_3+SiO_2) with a fixed Al_2O_3/SiO_2 weight ratio of 0.4 in the liquid. This Al_2O_3/SiO_2 weight ratio was selected based on the average compositions of the current blast furnace slags from Shougang [27]. The selection of CaO and MgO as the end members enables us to discuss the effect of flux composition on slag phase equilibrium.

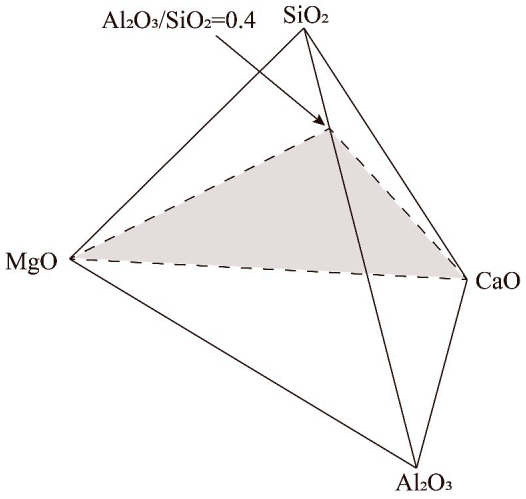


Figure 1. Presentation of the pseudo-ternary phase diagram in the CaO-MgO-(SiO_2+Al_2O_3) system at fixed Al_2O_3/SiO_2 weight ratio of 0.4.

The microstructures and phase compositions of the quenched samples were determined by EPMA. Anorthite ($CaO{\cdot}Al_2O_3{\cdot}2SiO_2$), cordierite ($2MgO{\cdot}2Al_2O_3{\cdot}5SiO_2$), dicalcium silicate ($Ca_2SiO_4$), melilite ($2CaO{\cdot}MgO{\cdot}2SiO_2$-$2CaO{\cdot}Al_2O_3{\cdot}SiO_2$), merwinite

($3CaO{\cdot}MgO{\cdot}2SiO_2$), MgO, mullite ($3Al_2O_3{\cdot}2SiO_2$), spinel ($MgO{\cdot}Al_2O_3$) and forsterite ($2MgO{\cdot}SiO_2$-$2CaO{\cdot}SiO_2$) were observed in the quenched samples. Typical backscattered SEM micrographs of the quenched samples are shown in Figure 2a–f. Figure 2a–e show the coexistence of liquid with anorthite, cordierite, spinel, Mg_2SiO_4 and melilite, respectively. Figure 2f–h show the coexistence of liquid with anorthite and Mg_2SiO_4, melilite and spinel, MgO and merwinite, respectively. It can be seen from the figures that rapid cooling enabled the liquid to be converted to the uniform glass. All solid phases have a sharp edge and large enough size for EPMA measurements.

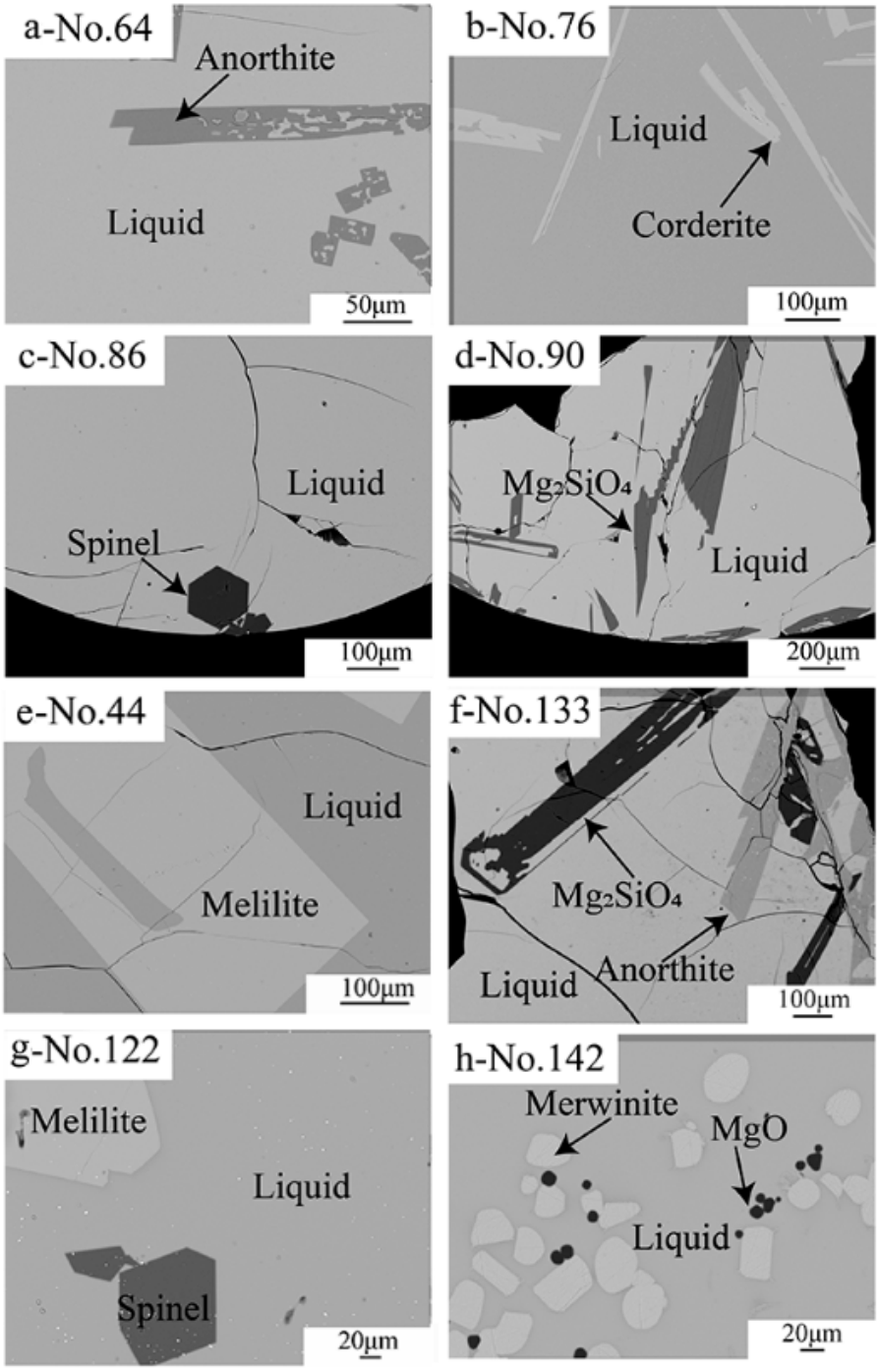


Figure 2. Typical backscattered SEM micrographs of the quenched slags showing the equilibrium of liquid with (**a**) anorthite, (**b**) cordierite, (**c**) spinel, (**d**) Mg_2SiO_4, (**e**) mellite, (**f**) Mg_2SiO_4 and anorthite, (**g**) melilite and spinel, (**h**) MgO and merwinite.

Initial compositions of the sample used in the high temperature experiments was presented in Table A1. The compositions of the phases measured by EPMA are given in Table A2 (weight%) and Table A3 (mol%). The experimental data from previous studies [15–18,23] using the same technique are also present in the Table A1. The compositions of the anorthite, dicalcium silicate, merwinite, MgO, mullite, forsterite and spinel are close to their stoichiometry with limited solid solutions. Melilite is the solid solution between akermanite ($2CaO{\cdot}MgO{\cdot}2SiO_2$) and gehlenite ($2CaO{\cdot}Al_2O_3{\cdot}SiO_2$). Cordierite is the solid solution between $2MgO{\cdot}2Al_2O_3{\cdot}5SiO_2$ and $2CaO{\cdot}2Al_2O_3{\cdot}5SiO_2$. The solubilities of the solid phases are summarized below:

Anorthite ($CaO{\cdot}Al_2O_3{\cdot}2SiO_2$): contains 24.5–25.3 mol% CaO, 0.3–1.1 mol% MgO, 23.1–24.7 mol% Al_2O_3 and 49.8–51.3 mol% SiO_2. The $SiO_2/(Al_2O_3+CaO+MgO)$ molar ratio is around 1.0 in the anorthite.

Dicalcium silicate (Ca_2SiO_4): up to 3.7 wt% MgO is present in the dicalcium silicate, the $(CaO+MgO)/SiO_2$ molar ratio varies from 1.99 to 2.04.

Merwinite ($3CaO{\cdot}MgO{\cdot}2SiO_2$): the CaO/MgO molar ratios vary in the range of 4.02–4.24 and MgO/SiO_2 molar ratios vary in the range of 0.33–0.38 in the merwinite.

MgO: up to 0.3 wt% CaO and 1.2 wt% Al_2O_3 are present in the MgO. Unexpectedly, more Al_2O_3 than CaO is present in the MgO.

Mullite ($3Al_2O_3{\cdot}2SiO_2$): up to 0.3 wt% CaO and 0.4 wt% MgO are present in the mullite. The molar ratio of Al_2O_3 to SiO_2 is up to 1.68.

Spinel ($MgO{\cdot}Al_2O_3$): up to 0.3 wt% CaO and 0.4 wt% SiO_2 are present in the spinel. The molar ratio of Al_2O_3 to MgO is up to 1.62.

Forsterite (Mg_2SiO_4): up to 4.2 wt% CaO and 0.5 wt% Al_2O_3 are present in the forsterite. The molar ratio of (CaO+MgO) to SiO_2 is 1.91–2.04.

Melilite: the molar ratio of akermanite ($2CaO{\cdot}MgO{\cdot}2SiO_2$) to gehlenite ($2CaO{\cdot}Al_2O_3{\cdot}SiO_2$) in the melilite phase varies from 0 to 5.59.

Cordierite: $2MgO{\cdot}2Al_2O_3{\cdot}5SiO_2$ was initially reported to be a compound in the system MgO-Al_2O_3-SiO_2 [28]. In the later studies of the system CaO-SiO_2-Al_2O_3-MgO, the cordierite primary phase field was reported again in the high-MgO and high-Al_2O_3 sections [10–13]. However, both the experimental studies and FactSage predictions did not mention the solubility of CaO in the $2MgO{\cdot}2Al_2O_3{\cdot}5SiO_2$. $2CaO{\cdot}2Al_2O_3{\cdot}5SiO_2$ phase was not reported in the literature. In the present study, four experiments (74–77) reported the exitance of the cordierite in equilibrium with liquid at high temperature. Analysis of the EPMA measurements shows that the cordierite was composed of CaO 21.3–22.7, MgO 0.4–0.8, Al_2O_3 21.4–22.8 and SiO_2 53.7–56.8 mol%. The $SiO_2/(Al_2O_3+CaO+MgO)$ molar ratio in the cordierite is around 1.25 which is higher than that in the anorthite. Figure 2b shows a typical microstructure of cordierite in a quenched sample where the solid phase is lighter than the liquid phase. In contrast, it can be seen from Figure 2a that the anorthite is darker than the liquid phase confirming that cordierite is a phase different from the anorthite although they have close compositions. The new information will provide useful information to develop a cordierite solid solution in the thermodynamic database.

The experimental data given in Table A1 have been used to construct the pseudo-ternary section (Al_2O_3+SiO_2)-CaO-MgO as shown in Figure 3. The boundaries were drawn by passing through the three phase points where liquid was in equilibrium with two solid phases (Exp No. 121–158). If three phase points were not available, the boundaries were drawn between the experimental points in different primary phase fields. It can be seen from the figure that most of the experimental points are in the primary phase fields of anorthite, melilite, forsterite, MgO, mullite and dicalcium silicate. The solid symbols are the liquid compositions determined in the present study and the open symbols are the liquid compositions reported in the previous studies using the same technique. The thin solid thin lines represent experimentally determined isotherms and the dashed thin lines represent the estimated isotherms. The thick lines represent the boundaries between the primary phase fields.

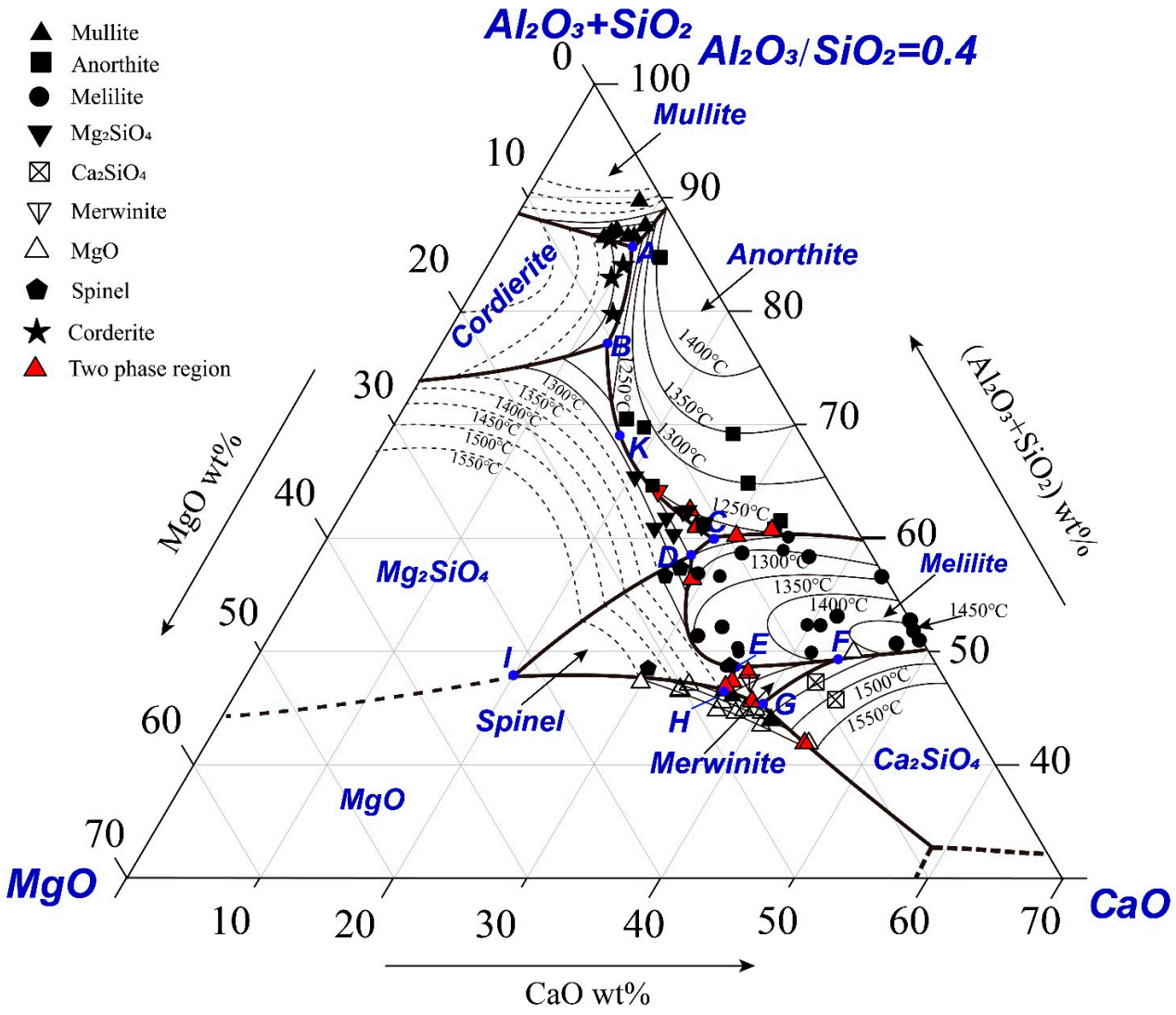


Figure 3. Experimentally determined pseudo-ternary phase diagram (SiO_2+Al_2O_3)-MgO-CaO with Al_2O_3/SiO_2 weight ratio of 0.4.

Nine special points in the system are estimated according to the boundaries and isothermals, as shown in Figure 4. The compositions and temperatures of the special points are given in Table 1. Point K on the boundary line BC joining the primary phase fields of anorthite and forsterite represents a local maximum temperature (1260 ± 5 °C). Experimental results reported by Osborn et al. [10] and Cavalier et al. [12] are shown in Figure 4 for comparison. The number next to the symbol is the liquidus temperature reported. The primary phases reported by Osborn et al. [10] show general agreement with the present results; however, the liquidus temperatures reported by Osborn et al. [10] are lower than the present results in some areas. Two points reported by Cavalier et al. [12] are shown in the figure. The point in the cordierite primary phase field agrees with the present result. However, another point was reported in the anorthite primary phase field with the liquidus temperature of 1272 °C by Cavalier et al. [12] which is in the forsterite primary phase field with the liquidus temperature of 1350 °C according to the present study.

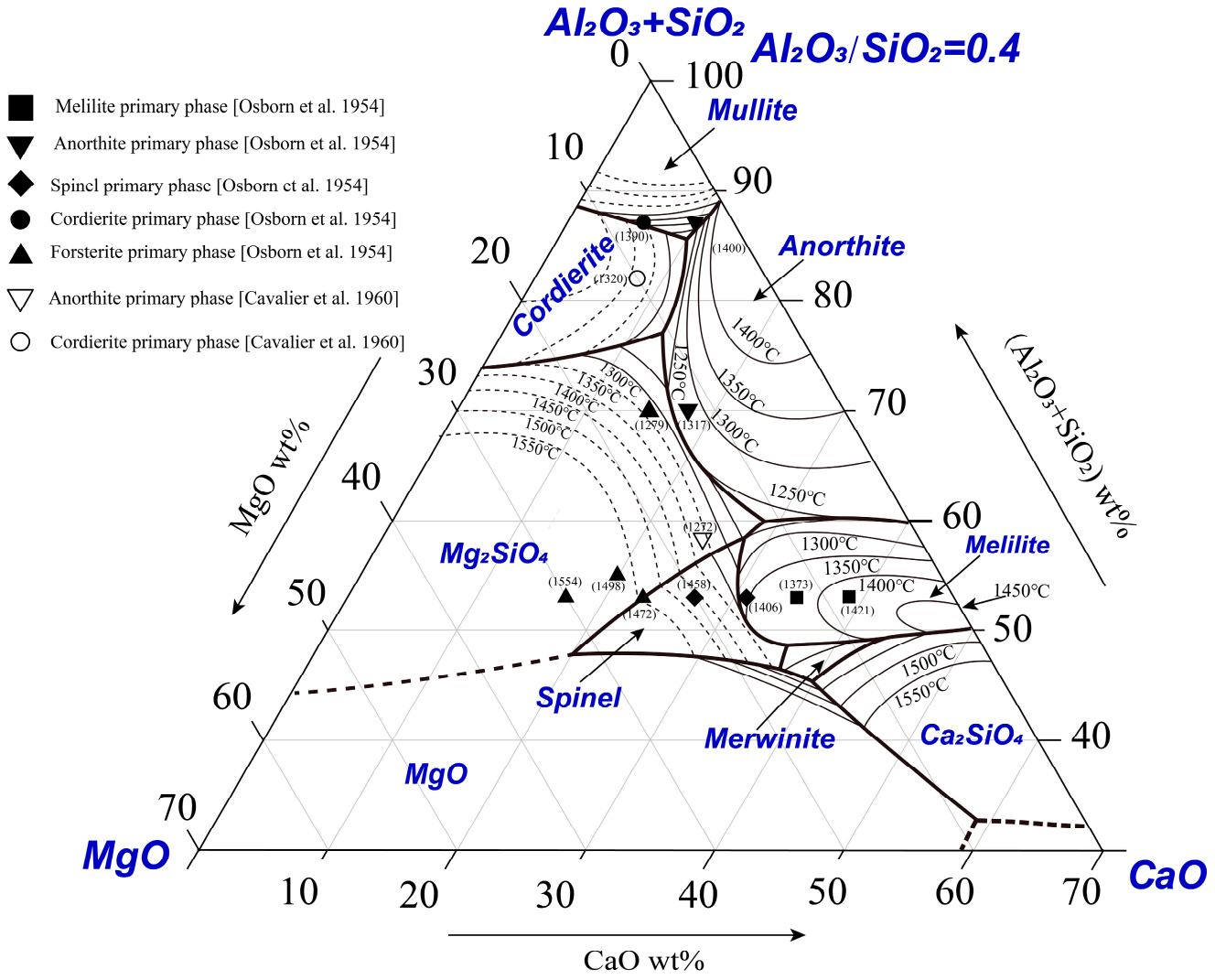


Figure 4. Comparison of the present results with the literature data [10,12].

Table 1. Estimated compositions and temperatures of the special points in the CaO-MgO-Al_2O_3-SiO_2 system with Al_2O_3/SiO_2 weight ratio of 0.4.

Special Point	Description	T (°C)	Composition (wt%)			
			CaO	MgO	Al_2O_3	SiO_2
A	L + mullite ↔ cordierite + anorthite	1250 (±5)	7.6	6.6	24.5	61.3
B	L ↔ cordierite + anorthite + Mg_2SiO_4	1240 (±10)	10.0	14.3	21.6	54.1
C	L ↔ melilite + anorthite + Mg_2SiO_4	1235 (±5)	27.5	11.6	17.4	43.6
D	L + spinel ↔ Mg_2SiO_4 + melilite	1270 (±10)	28.2	13.3	16.7	41.8
E	L + merwinite ↔ melilite + spinel	1380 (±10)	37.2	14.0	14.0	34.9
F	L + melilite + Ca_2SiO_4 ↔ merwinite	1455 (±5)	45.6	4.5	14.3	35.7
G	L + Ca_2SiO_4 ↔ merwinite + MgO	1480 (±10)	36.7	16.6	13.3	33.3
H	L + MgO ↔ merwinite + spinel	1410 (±10)	43.1	13.2	12.5	31.2
I	L + MgO + Mg_2SiO_4 ↔ + spinel	1650 (±20)	20.0	32.1	13.7	34.2

3.2. Application of Phase Diagram in Ironmaking Process

Pseudo-binary phase diagrams are often used by operators and researchers to discuss the effect of slag composition on liquidus temperatures. A typical composition of Shougang BF slag [27] is shown in Figure 5. It can be seen that the BF composition is in the melilite primary phase field with the liquidus temperature 1400–1450 °C. Shougang has a stable supply of raw materials for the BF, resulting a relative stable Al_2O_3/SiO_2 weight ratio of 0.4

in the slag. The additions of MgO and CaO can be adjusted according to the requirements. It is more convenient to use a pseudo-binary phase diagram to discuss the effect of a single parameter on liquidus temperature. The red line, as shown in Figure 5, indicates how the pseudo-binary phase diagrams are interpolated from the pseudo-ternary phase diagram. Based on the pseudo-ternary phase diagram determined, the effects of MgO/CaO, and quaternary basicity (CaO+MgO)/(Al_2O_3+SiO_2) on the liquidus temperature can be considered from different directions, as shown in Figure 5.

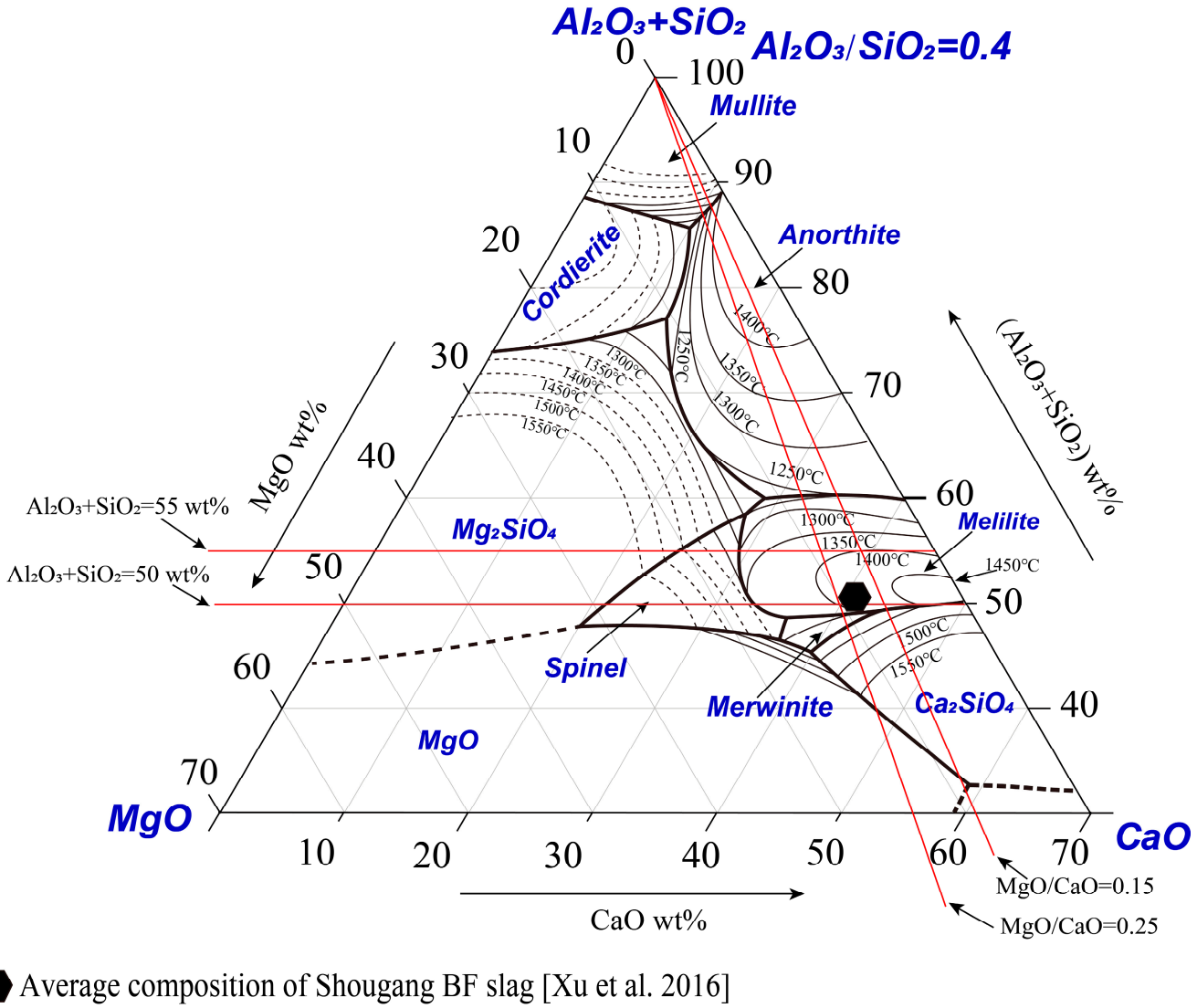


Figure 5. A typical composition of Shougang blast furnace slag [27] and effects of slag composition on the liquidus temperature.

3.2.1. Effect of MgO/CaO Weight Ratio on Liquidus Temperature

Figure 6 shows the liquidus temperatures as a function of MgO/CaO weight ratio in liquid at fixed (Al_2O_3+SiO_2) of 50 and 55 wt%, respectively. The typical composition of Shougang BF slag and FactSage predictions are also shown in the figure. It can be seen that melilite is the primary phase at low MgO/CaO weight ratio and spinel is the primary phase at high MgO/CaO weight ratio. The liquidus temperatures decrease in the melilite primary phase field and increase in the spinel primary phase field with increasing MgO/CaO weight ratio. In both melilite and spinel primary phase fields, higher (Al_2O_3+SiO_2) concentration (55 wt%) results in a lower liquidus temperature at a given MgO/CaO weight ratio. It is possible to decrease the liquidus temperature of the BF slag by increasing the MgO/CaO

weight ratio up to 0.52. However, there is a limitation for the MgO/CaO ratio where the primary phase changes to the spinel. In comparison between the experimental results and FactSage predictions, it can be seen that the sizes of the melilite and spinel primary phase fields determined in the present study are much larger than the FactSage predictions. For example, FactSage predicts the MgO primary phase field when the MgO/CaO weight ratio is higher than 0.93. However, the MgO primary phase only appears from MgO/CaO weight ratio 1.39 according to the experimental results. Nearly 100 °C difference of the liquidus temperature occurs between the experimental results and FactSage predictions at MgO/CaO ratio 0.52.

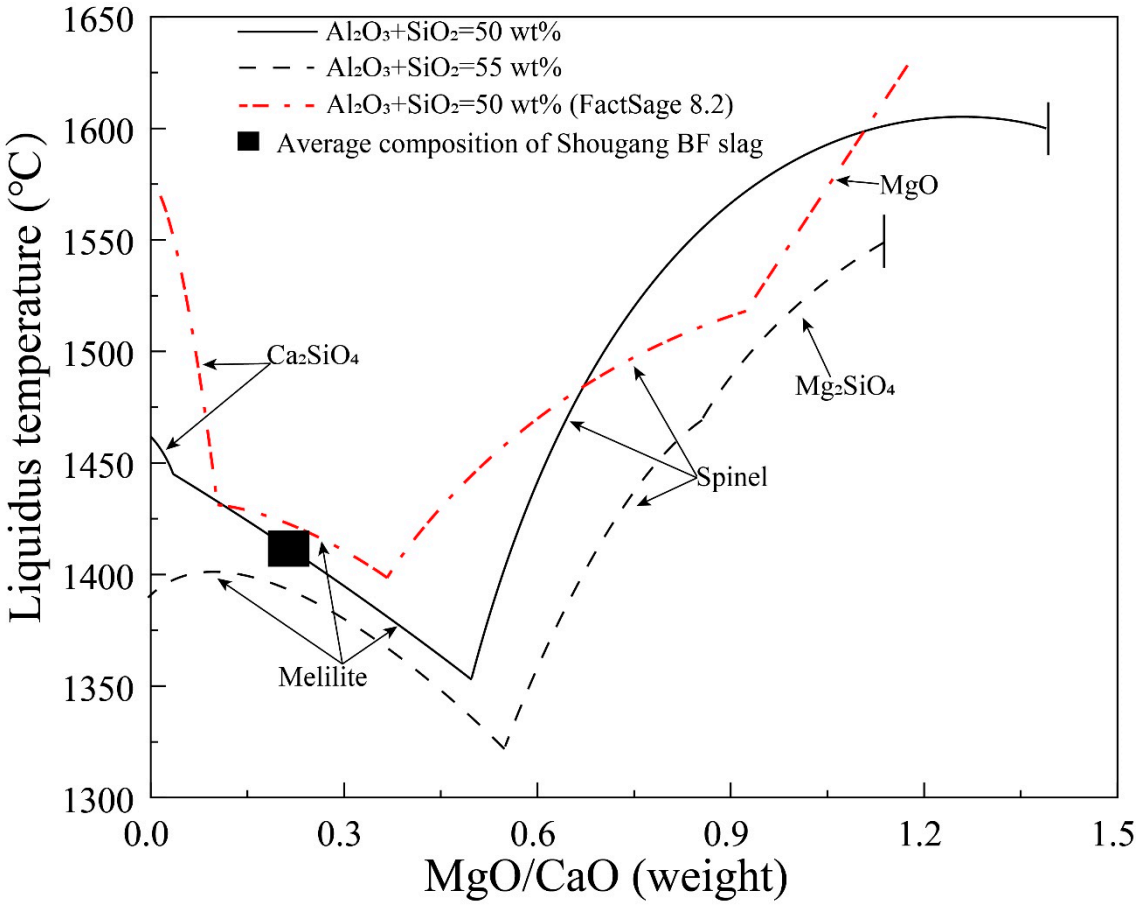


Figure 6. Liquidus temperature as a function of MgO/CaO in liquids at fixed (Al_2O_3+SiO_2) of 50 and 55 wt% in the CaO-MgO-SiO_2-Al_2O_3 system with Al_2O_3/SiO_2 weight ratio of 0.4.

3.2.2. Effect of Quaternary Basicity on Liquidus Temperature

Due to the significant impact of the concentrations of Al_2O_3 and MgO in slag on the actual basicity and desulfurization capacity of the BF slag, the CaO/SiO_2 binary basicity cannot reflect the basicity of high Al_2O_3 slag objectively [5]. Therefore, the desulfurization coefficient or capacity is more closely related to quaternary basicity (CaO+MgO)/(SiO_2+Al_2O_3). It is worth noting that the quaternary basicity will be forced to increase when the magnesium flux pellet is widely used in the blast furnace, which can greatly affect the softening–melting properties of burden materials in the cohesive zone [7]. Hence, it is necessary to understand the effect of quaternary basicity on the liquidus temperature of the BF slags. Figure 7 shows the liquidus temperature as a function of (CaO+MgO)/(SiO_2+Al_2O_3) in liquids at fixed MgO/CaO weight ratios of 0.15 and 0.25. FactSage predictions are also shown in the figure for comparison. As can be seen, mullite, anorthite, melilite, merwinite and Ca_2SiO_4 are the primary phases in the composition range investigated. The quaternary basicity has a significant influence on the liquidus temperatures of all primary phase fields.

The typical Shougang BF slag composition is in the melilite primary phase field close to the merwinite (MgO/CaO = 0.25) or Ca_2SiO_4 (MgO/CaO = 0.15) primary phase field. Decrease of the quaternary basicity from the current slag composition can decrease the liquidus temperature significantly. Further increase of the quaternary basicity will bring the slag into the merwinite or Ca_2SiO_4 primary phase fields causing significant increase of the liquidus temperature. It can be seen that increase of the MgO/CaO ratio from 0.15 to 0.25 can slightly decrease the liquidus temperature in the anorthite and melilite primary phase fields but significantly decrease the liquidus temperature in the Ca_2SiO_4 primary phase field. In conclusion, the Shougang BF slag with a quaternary basicity of 1.05 has the optimum composition at the MgO/CaO weight ratio 0.15. If the MgO/CaO weight ratio is increased to 0.25, the quaternary basicity can be further increased, which will decrease the liquidus temperature and increase the desulfurization capacity. The predicted liquidus temperatures in the anorthite and Ca_2SiO_4 primary phase fields are close to the experimental results. In the melilite primary phase field, there is up to 50 °C difference between the FactSage predictions and experimental results. Experimentally determined merwinite phase is not predicted by FactSage.

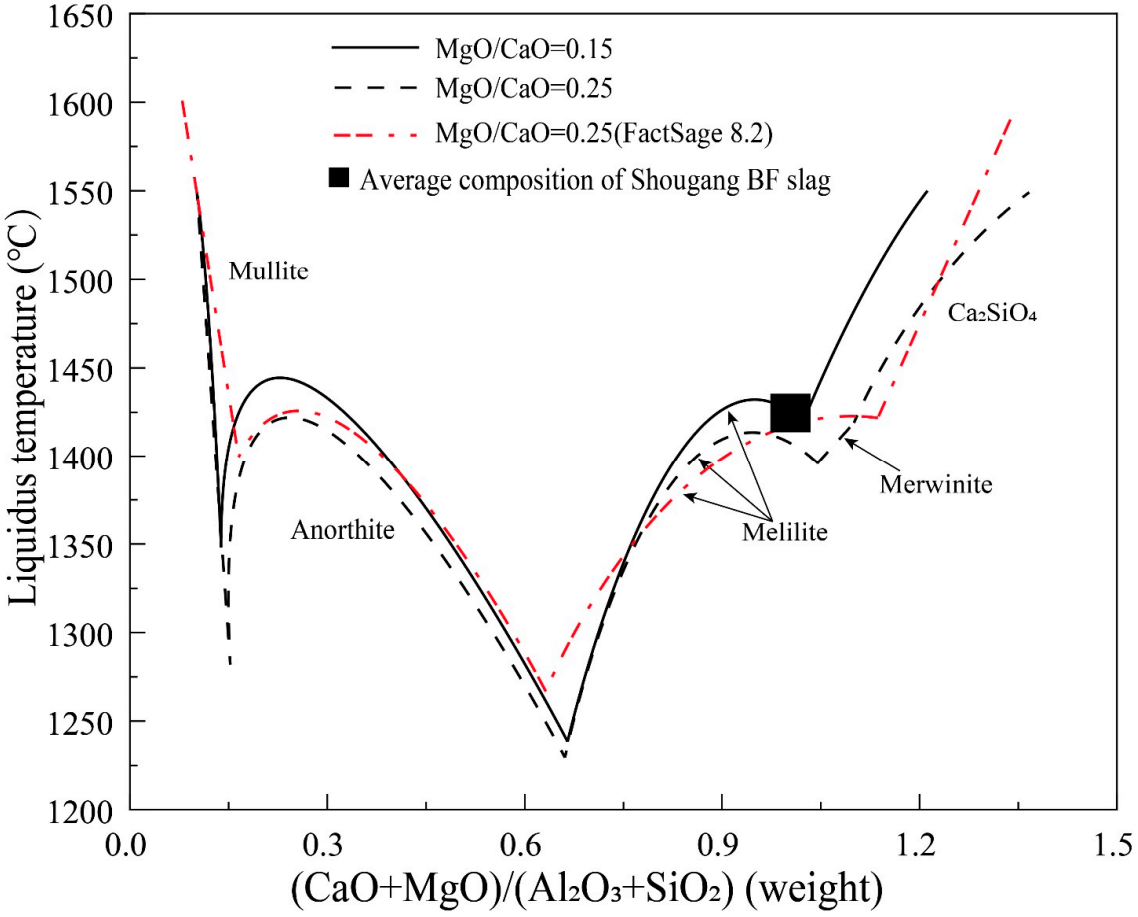


Figure 7. Liquidus temperature as a function of quaternary basicity in liquid at fixed MgO/CaO weight ratios of 0.15 and 0.25 in the CaO-MgO-SiO_2-Al_2O_3 system with Al_2O_3/SiO_2 weight ratio of 0.4.

3.3. Comparison of Experimental Data and FactSage Predictions

FactSage is one of the most successful thermodynamic models in predicting the liquidus temperatures of oxide slags [25]. Accurate experimental data can be used to evaluate the accuracy of the FactSage predictions and support the optimization of the existing database and new database development. Clarifying the difference between the calculated and experimental data is of great significance for optimizing thermodynamic database and avoiding misleading industrial practices. As shown in Figures 6 and 7, a

significant difference occurs on the primary phase and the liquidus temperatures between the FactSage predictions and experimental results.

As discussed above, the current composition of the Shougang blast furnace slag is usually in the melilite primary phase field as shown in Figures 6 and 7. Melilite is the solid solution between akermanite ($2CaO{\cdot}MgO{\cdot}2SiO_2$) and gehlenite ($2CaO{\cdot}Al_2O_3{\cdot}SiO_2$). Figure 8 presents the comparison of the experimental data and FactSage predictions. The experiments No. 44–63 listed in Table A1 were used to calculate the primary phases and their liquidus temperatures by FactSage 8.2. Melilite is the primary phase in experiments No. 44–63. However, it can be seen from Figure 8 that anorthite, spinel and Ca_2SiO_4 are also predicted by the FactSage in addition to melilite. Up to 75 °C difference of the liquidus temperature is observed between the predictions and experimental results.

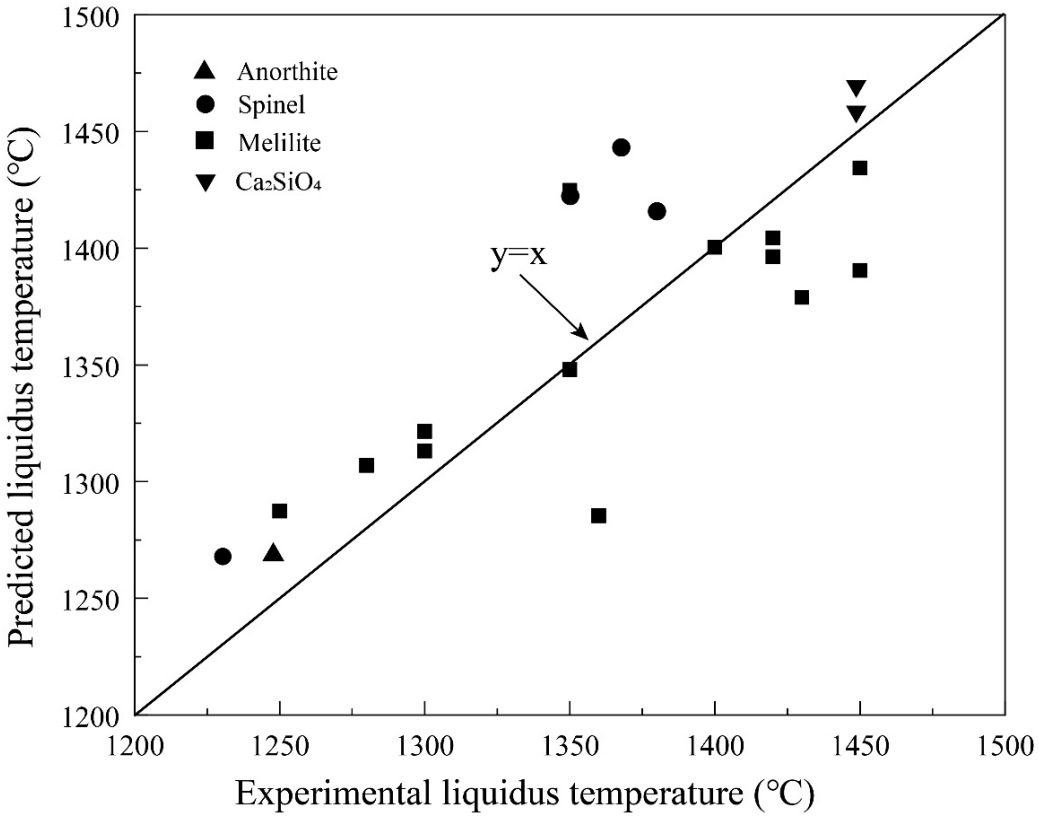


Figure 8. Comparison of the experimental results and FactSage predictions on primary phase and liquidus temperatures. All experimental liquidus are in the melilite primary phase field. The predicted primary phases are shown in the figure.

The experiments No. 99–100 listed in Table A1 show that Mg_2SiO_4 is the primary phase in the quenched samples. The liquid compositions of these samples were used to calculate the primary phase and liquidus temperatures and the results are shown in Table 2. It can be seen that anorthite, spinel, melilite and merwinite are predicted by the FactSage showing that the current database needs to be optimized. The discrepancies between the experimental and predicted liquidus temperatures are up to 112 °C.

Table 3 shows the comparison of the experimental results and FactSage predictions where merwinite is the primary phase of the experiments No. 115–119. FactSage predicted melilite, MgO and spinel as the primary phases but no merwinite. The liquidus temperature predicted by FactSage 8.2 is 189 °C higher than the experimental data (No. 117). Lack of accurate experimental data in the composition range causes inaccuracy in the thermodynamic database.

Table 2. Comparison of the experimental data with the FactSage predictions on primary phase and liquidus temperature, Mg_2SiO_4 is the primary phase in all experiments.

Exp. No.	Experimental Liquidus Temperature (°C)	Liquid Composition (wt%)				Predicted Liquidus Temperature (°C)	Predicted Primary Phase
		CaO	MgO	Al_2O_3	SiO_2		
90	1250	25.8	11.6	18.7	44.0	1287	Anorthite
91	1250	27.6	11.7	17.2	43.5	1258	Spinel
92	1250	26.9	11.8	18.1	42.8	1287	Spinel
93	1300	20.5	14.4	18.5	46.6	1294	Anorthite
94	1300	24.6	13.9	18.2	43.2	1315	Spinel
95	1300	25.9	14.1	17.3	42.7	1307	Spinel
96	1300	40.9	11.6	7.9	39.6	1412	Merwinite
97	1330	24.2	15.3	17.8	42.7	1333	Spinel
98	1350	29.2	16.6	14.0	40.1	1325	Melilite
99	1400	27.7	18.5	13.7	40.0	1342	Mg_2SiO_4
100	1400	28.0	14.7	15.8	41.4	1306	Spinel

Table 3. Comparison of the experimental data with the FactSage prediction on primary phase and liquidus temperature; merwinite is the primary phase in all experiments.

Exp. No.	Experimental Liquidus Temperature (°C)	Liquid Composition (wt%)				Predicted Liquidus Temperature (°C)	Predicted Primary Phase
		CaO	MgO	Al_2O_3	SiO_2		
115	1400	41.1	8.9	14.7	35.3	1427	Melilite
116	1400	37.9	14.2	13.1	34.7	1421	Spinel
117	1430	39.8	15.7	13.4	31.1	1619	MgO
118	1450	40.1	15.1	13.1	31.7	1555	MgO
119	1450	43.1	9.6	13.8	33.4	1425	Melilite

4. Conclusions

The phase equilibria in the CaO-MgO-SiO_2-Al_2O_3 system with an Al_2O_3/SiO_2 weight ratio of 0.4 have been experimentally investigated in the composition range related to blast furnace slags. A pseudo-ternary phase diagram (CaO+MgO)-SiO_2-Al_2O_3 has been constructed using the experimentally data. Pseudo-binary phase diagrams are used to discuss the effects of quaternary basicity and MgO/CaO weight ratio on liquidus temperatures of the blast furnace slags. The experimentally determined liquidus temperatures and solid solution compositions are compared with the FactSage predictions to provide useful information for optimization of the thermodynamic database.

Author Contributions: Methodology, B.Z.; Validation, B.Z.; Formal analysis, J.L.; Investigation, J.L. and G.Q.; Resources, G.Q.; Data curation, J.L.; Writing—original draft, J.L. and G.Q.; Writing—review & editing, B.Z.; Supervision, B.Z.; Project administration, B.Z. All authors have read and agreed to the published version of the manuscript.

Funding: This research received no external funding.

Data Availability Statement: Not applicable.

Acknowledgments: The authors would like to acknowledge Shougang Research Institute of Technology for providing the financial support.

Conflicts of Interest: The authors declare that they have no conflict of interest.

Appendix A

Table A1. Initial compositions of the sample used in the high temperature experiments.

No.	Composition (wt%)			
	CaO	**MgO**	**Al_2O_3**	**SiO_2**
M1	31.3	6.3	17.9	44.5
M2	41.7	8.3	14.3	35.7
M3	37.0	7.4	15.9	39.7
M4	45.4	9.1	13.0	32.5
M5	27.8	5.6	19.0	47.6
M6	39.3	7.9	15.1	37.7
M7	34.3	6.9	16.8	42.0
M8	25.6	5.1	19.8	49.5
M9	12.4	2.5	24.3	60.8
M10	10.4	2.1	25.0	62.5
M11	6.3	1.3	26.4	66.0
M12	9.0	1.8	25.5	63.7
M13	32.5	20.5	14.0	33.0
M14	14.7	2.9	30.9	51.5
M15	27.8	5.6	25.0	41.6
M16	11.4	4.6	24.0	60.0
M17	7.9	3.2	25.4	63.5
M18	9.4	3.8	24.8	62.0
M19	22.1	8.9	19.7	49.3
M20	28.5	11.4	17.2	42.9
M21	35.4	14.2	14.4	36.0
M22	36.4	14.6	14.0	35.0
M23	39.4	15.8	12.8	32.0
M24	42.9	17.1	11.4	28.6
M25	32.1	12.9	15.7	39.3
M26	25.3	10.1	18.4	46.2
M27	34.9	25.1	11.4	28.6
M28	29.1	20.9	14.3	35.7
M29	23.3	16.7	17.1	42.9
M30	32.0	23.0	12.8	32.2
M31	26.7	19.2	15.4	38.7
M32	20.4	14.7	18.6	46.3
M33	30.5	21.9	13.6	34.0
M34	16.6	12.0	20.4	51.0
M35	9.7	7.0	23.8	59.5
M36	5.8	4.2	25.7	64.3
M37	35.4	21.2	12.4	31.0
M38	25.3	15.2	17.0	42.5
M39	7.8	4.7	25.0	62.5
M40	10.0	6.0	24.0	60.0
M41	18.8	11.3	20.0	49.9
M42	21.9	13.1	18.6	46.4
M43	23.0	13.8	18.1	45.1
M44	26.9	16.1	16.3	40.7
M45	31.3	18.8	14.3	35.6
M46	37.5	22.5	11.4	28.6
M47	33.6	20.2	13.2	33.0
M48	24.0	14.4	17.6	44.0
M49	12.5	7.5	22.8	57.2
M50	5.6	3.4	26.0	65.0
M51	16.4	6.6	22.0	55.0
M52	7.7	5.6	24.8	61.9

Table A2. Experimental Results in the System CaO-MgO-Al_2O_3-SiO_2 system with Al_2O_3/SiO_2 weight ratio of 0.4.

Mixture				Compositions (wt%)				
No.	**No.**	**T (°C)**	**Phases**	**CaO**	**MgO**	**Al_2O_3**	**SiO_2**	**Al_2O_3/SiO_2**
				Liquid only				
M20	1	1250	Liquid	28.9	11.5	17.3	42.3	0.41
M26	2	1250	Liquid	27.1	9.6	19.7	43.6	0.45
M34	3	1250	Liquid	16.5	12.1	20.4	51.0	0.40
M16	4	1280	Liquid	11.6	4.6	23.8	60.0	0.40
M16	5	1300	Liquid	11.6	4.5	24.0	59.9	0.40
M34	6	1300	Liquid	16.4	12.1	20.3	51.2	0.40
M35	7	1300	Liquid	9.6	7.0	23.3	60.1	0.39
M36	8	1300	Liquid	6.8	4.9	21.5	66.8	0.32
M42	9	1300	Liquid	22.6	12.7	18.9	45.8	0.41
M48	10	1300	Liquid	24.8	14.0	18.0	43.2	0.42
M42	11	1310	Liquid	22.2	13.2	18.7	45.9	0.41
M19	12	1320	Liquid	22.7	9.0	19.7	48.6	0.41
M42	13	1320	Liquid	24.3	13.9	17.9	43.9	0.41
M25	14	1330	Liquid	31.6	13.0	15.9	39.5	0.40
M25	15	1330	Liquid	32.6	12.0	16.2	39.2	0.41
M48	16	1340	Liquid	22.9	12.6	19.3	45.2	0.43
M13	17	1350	Liquid	32.9	20.2	13.5	33.4	0.40
M16	18	1350	Liquid	11.6	4.5	23.6	60.3	0.39
M19	19	1350	Liquid	22.1	8.7	19.9	49.3	0.40
M25	20	1350	Liquid	31.9	12.8	15.6	39.7	0.39
M51	21	1350	Liquid	17.9	6.8	23.1	52.2	0.44
M51	22	1350	Liquid	18.5	7.3	23.8	50.4	0.47
M29	23	1350	Liquid	23.2	16.7	17.2	42.9	0.40
M42	24	1350	Liquid	24.4	12.3	20.3	43.0	0.47
M44	25	1350	Liquid	26.7	16.4	16.4	40.5	0.40
M49	26	1350	Liquid	12.9	7.6	23.1	56.4	0.41
M16	27	1350	Liquid	11.5	4.6	23.9	60.0	0.40
M35	28	1350	Liquid	9.9	7.0	23.9	59.2	0.40
M22	29	1390	Liquid	36.5	14.4	14.1	35.0	0.40
M22	30	1400	Liquid	36.5	14.0	13.7	35.8	0.38
M28	31	1400	Liquid	29.8	21.0	14.2	35.0	0.41
M41	32	1400	Liquid	20.9	11.9	22.5	44.7	0.50
M49	33	1400	Liquid	14.7	8.4	25.4	51.5	0.49
M21	34	1400	Liquid	35.6	14.2	14.5	35.7	0.41
M23	35	1450	Liquid	38.7	14.1	12.8	34.4	0.37
M23	36	1450	Liquid	39.4	15.7	12.8	32.1	0.40
M47	37	1450	Liquid	33.8	18.9	13.2	34.1	0.39
M23	38	1450	Liquid	38.8	15.4	13.6	32.2	0.42
M14	39	1480	Liquid	15.0	2.9	30.6	51.5	0.59
M14	40	1500	Liquid	15.0	3.0	30.5	51.5	0.59
M23	41	1500	Liquid	39.5	15.8	12.9	31.8	0.40
M30	42	1500	Liquid	45.0	1.1	17.9	36.0	0.50
M47	43	1500	Liquid	33.9	19.1	13.5	33.5	0.40
				Liquid + Melilite				
M20	44	1230	Liquid	27.7	11.4	17.7	43.2	0.41
			melilite	41.0	12.1	6.4	40.5	
M7	45	1250	Liquid	33.0	6.2	17.6	43.2	0.41
			melilite	41.1	10.4	10.4	38.1	
M43	46	1250	Liquid	27.4	11.3	17.9	43.4	0.41
			melilite	40.5	12.4	5.8	41.3	
	47 *	1280	Liquid	31.7	9.5	16.3	42.5	0.38
			melilite	8.8	40.6	39.1	11.5	

Table A2. *Cont.*

Mixture				Compositions (wt%)				
No.	**No.**	**T (°C)**	**Phases**	**CaO**	**MgO**	**Al_2O_3**	**SiO_2**	**Al_2O_3/SiO_2**
M7	48	1300	Liquid	34.5	6.5	16.6	42.4	0.39
			melilite	41.7	8.4	12.4	37.5	
	49 *	1300	Liquid	37.0	4.7	16.6	41.7	0.40
			melilite	32.9	41.0	18.7	7.4	
M21	50	1350	Liquid	31.8	16.8	14.7	36.7	0.40
			melilite	41.1	9.6	13.2	36.1	
M17	51	1350	Liquid	8.6	3.5	23.4	64.5	0.36
			melilite	0.1	0.2	73.1	26.6	
M3	52	1350	Liquid	36.4	7.2	15.4	41.0	0.37
			melilite	41.0	8.3	15.8	34.9	
	53 *	1360	Liquid	43.2	0.0	16.3	40.5	0.40
			melilite	40.6	0.0	36.6	22.8	
M22	54	1370	Liquid	35.3	15.9	13.7	35.1	0.39
			melilite	40.8	8.6	16.1	34.5	
M21	55	1380	Liquid	35.4	14.2	14.7	35.7	0.41
			melilite	41.7	8.0	16.6	33.7	
M6	56	1400	Liquid	39.5	8.0	14.6	37.9	0.39
			melilite	41.6	5.6	22.6	30.2	
	57 *	1420	Liquid	41.6	5.1	15.3	38.0	0.40
			melilite	41.2	3.9	27.0	27.9	
	58 *	1420	Liquid	40.9	6.8	14.7	37.6	0.39
			melilite	41.0	5.1	24.3	29.6	
	59 *	1430	Liquid	47.4	0.0	15.1	37.5	0.40
			melilite	41.4	0.0	36.4	22.2	
	60 *	1450	Liquid	44.6	5.4	14.5	35.5	0.41
			melilite	41.1	2.8	29.8	26.3	
	61 *	1450	Liquid	48.0	0.0	14.9	37.1	0.40
			melilite	41.0	0.0	36.9	22.1	
	62 *	1450	Liquid	47.4	2.0	14.1	36.5	0.39
			melilite	41.0	1.4	33.4	24.2	
	63 *	1450	Liquid	48.9	0.0	14.4	36.7	0.39
			melilite	40.9	0.0	37.2	21.9	
				Liquid + Anorthite				
M26	64	1250	Liquid	27.7	11.3	17.0	44.0	0.39
			Anorthite	20.3	0.2	35.4	44.1	
M35	65	1250	Liquid	32.1	6.7	16.3	44.9	0.36
			Anorthite	20.2	0.3	35.8	43.7	
M43	66	1280	Liquid	22.0	13.3	18.3	46.4	0.39
			Anorthite	20.2	0.4	35.6	43.8	
	67 *	1280	Liquid	33.4	5.2	16.8	44.6	0.38
			Anorthite	36.1	43.4	20.3	0.2	
M34	68	1290	Liquid	17.2	12.4	20.6	49.8	0.41
			Anorthite	20.1	0.6	34.5	44.8	
M41	69	1300	Liquid	18.6	11.5	19.5	50.4	0.39
			Anorthite	20.0	0.6	34.4	45.0	
M19	70	1300	Liquid	22.3	9.7	17.4	50.6	0.35
			Anorthite	20.1	0.5	35.7	43.7	
M5	71	1300	Liquid	29.1	6.3	16.8	47.8	0.35
			Anorthite	20.5	0.3	36.0	43.2	
M8	72	1350	Liquid	26.1	5.3	18.8	49.8	0.38
			anorthite	20.4	0.3	35.6	43.7	
M9	73	1400	Liquid	12.3	2.6	23.5	61.6	0.38
			anorthite	19.8	0.2	36.3	43.7	
				Liquid + Cordierite				
M17	74	1250	Liquid	9.7	7.2	23.7	59.4	0.40
			Cordierite	18.0	0.5	32.6	48.9	

Table A2. *Cont.*

Mixture				Compositions (wt%)				
No.	**No.**	**T (°C)**	**Phases**	**CaO**	**MgO**	**Al_2O_3**	**SiO_2**	**Al_2O_3/SiO_2**
M49	75	1300	Liquid	11.7	8.5	21.8	58.0	0.38
			Cordierite	18.6	0.5	33.9	47.0	
M40	76	1300	Liquid	10.0	6.0	23.8	60.2	0.39
			Cordierite	18.3	0.3	33.6	47.8	
M10	77	1300	Liquid	9.9	2.4	24.5	63.2	0.39
			Cordierite	17.5	0.2	32.1	50.2	
				Liquid + Mullite				
M17	78	1250	Liquid	9.0	3.7	23.5	63.8	0.37
			Mullite	0.2	0.4	68.5	30.9	
M18	79	1320	Liquid	9.6	3.7	24.7	62.0	0.40
			Mullite	0.2	0.2	71.1	28.5	
M39	80	1350	Liquid	8.0	4.7	24.7	62.6	0.39
			Mullite	0.1	0.3	70.9	28.7	
M36	81	1400	Liquid	6.2	4.5	23.5	65.8	0.36
			Mullite	0.2	0.3	72.6	26.9	
M12	82	1400	Liquid	9.5	1.8	23.9	64.8	0.37
			Mullite	0.1	0.1	71.9	27.9	
M11	83	1450	Liquid	8.4	1.8	25.1	64.7	0.39
			Mullite	0.1	0.0	74.0	25.9	
M50	84	1500	Liquid	5.9	3.5	24.4	66.2	0.37
			Mullite	0.1	0.1	73.2	26.6	
				Liquid + Spinel				
M29	85	1320	Liquid	25.2	14.9	18.5	41.4	0.45
			Spinel	0.0	28.2	71.7	0.1	
M44	86	1350	Liquid	27.1	16.3	16.3	40.3	0.40
			Spinel	0.1	28.2	71.6	0.1	
M22	87	1370	Liquid	35.6	15.6	13.8	35.0	0.39
			Spinel	0.0	28.1	71.8	0.1	
	89 *	1500	liquid	30.4	21.7	14.1	33.8	0.42
			Spinel	0.3	0.4	70.9	28.4	
				Liquid + Mg_2SiO_4				
M48	90	1250	Liquid	25.8	11.6	18.7	43.9	0.42
			Mg_2SiO_4	1.0	56.9	0.1	42.0	
M38	91	1250	Liquid	27.6	11.7	17.2	43.5	0.40
			Mg_2SiO_4	1.6	55.8	0.1	42.5	
M44	92	1250	Liquid	27.0	11.8	18.2	43.0	0.42
			Mg_2SiO_4	1.4	56.4	0.4	41.8	
M32	93	1300	Liquid	20.5	14.4	18.5	46.6	0.40
			Mg_2SiO_4	0.6	56.7	0.1	42.6	
M29	94	1300	Liquid	24.6	13.9	18.2	43.3	0.42
			Mg_2SiO_4	1.1	56.4	0.3	42.2	
M38	95	1300	Liquid	25.9	14.1	17.3	42.7	0.41
			Mg_2SiO_4	1.3	56.0	0.2	42.5	
M28	96	1300	Liquid	40.9	11.6	7.9	39.6	0.20
			Mg_2SiO_4	4.2	53.8	0.2	41.8	
M29	97	1330	Liquid	24.2	15.3	17.8	42.7	0.42
			Mg_2SiO_4	1.1	56.6	0.2	42.1	
M31	98	1350	Liquid	29.2	16.6	14.0	40.2	0.35
			Mg_2SiO_4	2.4	55.2	0.5	41.9	
M31	99	1400	Liquid	27.7	18.5	13.7	40.1	0.34
			Mg_2SiO_4	2.6	55.1	0.3	42.0	
M44	100	1400	Liquid	28.0	14.7	15.8	41.5	0.38
			Mg_2SiO_4	0.6	56.7	0.1	42.6	
				Liquid + MgO				
M30	101	1450	Liquid	33.4	19.3	13.6	33.7	0.40
			MgO	0.2	98.9	0.9	0.0	

Table A2. *Cont.*

Mixture				Compositions (wt%)				
No.	**No.**	**T (°C)**	**Phases**	**CaO**	**MgO**	**Al_2O_3**	**SiO_2**	**Al_2O_3/SiO_2**
M23	102	1470	Liquid	39.5	15.5	12.8	32.2	0.40
			MgO	0.3	98.9	0.8	0.0	
	103 *	1500	Liquid	30.0	22.7	13.5	33.8	0.40
			MgO	0.1	0.2	1.2	98.5	
	104 *	1500	Liquid	41.4	14.6	12.3	31.7	0.39
			MgO	0.3	99.0	0.7	0.0	
M27	105	1500	Liquid	38.7	16.3	12.6	32.4	0.39
			MgO	0.2	99.0	0.8	0.0	
M30	106	1500	Liquid	32.9	20.3	13.5	33.3	0.40
			MgO	0.1	98.8	1.1	0.0	
M30	107	1500	Liquid	32.9	20.2	13.5	33.4	0.40
			MgO	0.2	98.7	1.1	0.0	
M30	108	1500	Liquid	32.9	20.3	13.5	33.3	0.40
			MgO	0.2	98.8	1.0	0.0	
M37	109	1500	Liquid	36.6	17.6	13.1	32.7	0.40
			MgO	0.3	98.8	0.9	0.0	
M27	110	1550	Liquid	38.1	17.1	12.8	32.0	0.40
			MgO	0.1	99.0	0.9	0.0	
M24	111	1550	Liquid	44.9	13.0	12.1	30.0	0.40
			MgO	0.3	99.1	0.6	0.0	
M46	112	1550	Liquid	41.1	14.8	12.6	31.5	0.40
			MgO	0.3	99.0	0.7	0.0	
M46	113	1550	Liquid	40.6	15.7	12.9	30.8	0.42
			MgO	0.3	98.9	0.8	0.0	
M37	114	1550	Liquid	36.6	18.4	12.8	32.2	0.40
			MgO	0.2	98.8	1.0	0.0	
				Liquid + Merwinite				
	115 *	1400	Liquid	38.0	14.2	13.1	34.7	0.38
			Merwinite	51.2	12.6	0.1	36.1	
M2	116	1400	Liquid	41.1	8.9	14.7	35.3	0.42
			Merwinite	51.1	12.2	0.1	36.6	
M23	117	1430	Liquid	39.8	15.7	13.4	31.1	0.43
			Merwinite	52.4	13.0	0.1	34.5	
	118 *	1450	Liquid	43.2	9.6	13.8	33.4	0.41
			Merwinite	51.3	12.1	0.1	36.5	
M23	119	1450	Liquid	40.1	15.1	13.1	31.7	0.41
			Merwinite	51.8	12.7	0.1	35.4	
				Liquid + Ca_2SiO_4				
M4	120	1500	Liquid	45.1	9.1	13.4	32.4	0.41
			Ca_2SiO_4	61.6	2.9	0.2	35.3	
				Liquid + Melilite + Spinel				
M25	121	1300	Liquid	29.2	13.8	16.2	40.8	0.40
			Melilite	40.9	10.0	11.5	37.6	
			Spinel	0.1	28.2	71.6	0.1	
M25	122	1320	Liquid	31.0	12.2	16.7	40.1	0.42
			Melilite	41.2	10.0	11.9	36.9	
			Spinel	0.1	28.5	71.3	0.1	
				Liquid + Melilite + Anorthite				
M15	123	1250	Liquid	30.4	9.3	17.6	42.7	0.41
			Anorthite	20.5	0.4	36.6	42.5	
			Melilite	41.1	11.0	9.5	38.4	
M1	124	1250	Liquid	32.1	6.8	16.5	44.6	0.37
			Anorthite	20.5	0.1	35.9	43.5	
			Melilite	40.9	11.4	7.3	40.4	

Table A2. *Cont.*

Mixture				Compositions (wt%)				
No.	**No.**	**T (°C)**	**Phases**	**CaO**	**MgO**	**Al_2O_3**	**SiO_2**	**Al_2O_3/SiO_2**
				Liquid + Melilite + Mg_2SiO_4				
M20	125	1220	Liquid	27.1	11.0	18.8	43.1	0.44
			Mg_2SiO_4	1.3	56.5	0.3	41.9	
			Melilite	40.8	11.7	7.0	40.5	
M25	126	1250	Liquid	27.2	12.9	17.9	42.0	0.43
			Mg_2SiO_4	1.6	56.3	0.2	41.9	
			Melilite	40.3	9.8	12.2	37.7	
M45	127	1300	Liquid	29.0	13.8	15.5	41.7	0.37
			Mg_2SiO_4	2.4	55.2	0.4	42.0	
			Melilite	40.7	9.9	12.1	37.3	
M44	128	1300	Liquid	25.4	14.2	12.6	47.8	0.56
			Mg_2SiO_4	40.7	11.0	8.6	39.7	
			Melilite	2.1	54.8	1.7	41.4	
M28	129	1350	Liquid	31.0	16.4	12.8	39.8	
			Mg_2SiO_4	40.9	11.9	6.8	40.4	
			Melilite	3.9	53.8	0.3	42.0	
M45	130	1350	Liquid	30.1	16.4	13.5	40.0	0.34
			Mg_2SiO_4	4.1	54.0	0.2	41.7	
			Melilite	40.3	12.5	7.1	40.1	
M45	131	1450	Liquid	34.0	15.9	10.4	39.7	0.34
			Mg_2SiO_4	4.1	53.5	0.4	42.0	
			Melilite	41.2	11.7	7.8	39.3	
				Liquid + Mg_2SiO_4 + Anorthite				
M42	132	1200	Liquid	23.2	15.3	13.9	47.6	0.29
			Anorthite	19.7	0.8	34.6	44.9	
			Mg_2SiO_4	1.2	56.5	0.2	42.1	
M42	133	1230	Liquid	22.8	13.4	17.5	46.3	0.38
			Anorthite	20.2	0.5	35.7	43.6	
			Mg_2SiO_4	0.8	57.0	0.1	42.1	
M20	134	1230	Liquid	25.9	11.9	17.2	45.0	0.38
			Anorthite	20.1	0.2	35.6	44.1	
			Mg_2SiO_4	0.9	56.2	0.3	42.6	
M34	135	1240	Liquid	16.2	12.1	15.6	56.1	0.28
			Anorthite	19.9	1.0	33.1	46.0	
			Mg_2SiO_4	0.3	57.2	0.1	42.4	
M34	136	1250	Liquid	17.4	13.0	15.8	53.8	0.29
			Anorthite	19.8	0.9	33.7	45.6	
			Mg_2SiO_4	0.3	57.0	0.1	42.6	
M41	137	1250	Liquid	16.5	13.0	15.8	54.7	0.29
			Anorthite	19.7	0.9	34.1	45.3	
			Mg_2SiO_4	0.5	57.2	0.1	42.2	
M42	138	1250	Liquid	26.9	11.8	17.4	43.9	0.40
			Anorthite	20.3	0.5	34.8	44.4	
			Mg_2SiO_4	0.8	56.6	0.2	42.4	
				Liquid + Mg_2SiO_4 + Spinel				
M28	139	1400	Liquid	31.5	20.0	11.3	37.2	0.30
			Spinel	0.0	28.1	71.5	0.4	
			Mg_2SiO_4	4.4	53.4	0.3	41.9	
M28	140	1400	Liquid	30.7	19.7	11.4	38.2	0.30
			Spinel	0.0	28.5	71.3	0.2	
			Mg_2SiO_4	4.7	53.5	0.3	41.5	
M28	141	1400	Liquid	30.8	19.7	11.8	37.7	0.31
			Spinel	0.0	28.1	71.5	0.4	
			Mg_2SiO_4	4.4	53.4	0.3	41.9	

Table A2. *Cont.*

Mixture				Compositions (wt%)				
No.	**No.**	**T (°C)**	**Phases**	**CaO**	**MgO**	**Al_2O_3**	**SiO_2**	**Al_2O_3/SiO_2**
				Liquid + Merwinite + MgO				
M23	142	1450	Liquid	38.8	15.4	13.6	32.2	0.42
			MgO	0.3	98.9	0.8	0.0	
			Merwinite	50.8	12.6	0.1	36.5	
				Liquid + MgO + Ca_2SiO_4				
M24	143	1550	Liquid	44.6	13.3	12.0	30.1	0.40
			Ca_2SiO_4	60.9	3.7	0.2	35.2	
			MgO	0.3	99.0	0.7	0.0	
M24	144	1550	Liquid	42.3	12.8	17.1	27.8	0.30
			Ca_2SiO_4	51.5	12.2	0.2	36.1	
			MgO	0.3	98.9	0.8	0.0	
				Liquid + MgO + Spinel				
M47	145	1430	Liquid	34.9	18.5	12.5	34.1	0.37
			Spinel	0.2	28.1	71.6	0.1	
			MgO	0.2	99.0	0.8	0.0	
M33	146	1450	Liquid	30.5	21.7	12.6	35.2	0.36
			Spinel	0.0	28.4	71.4	0.2	
			MgO	0.1	99.0	0.9	0.0	
				Liquid + Merwinite + Spinel				
	147 *	1400	Liquid	37.6	14.2	14.0	34.2	0.41
			Spinel	0.1	28.0	71.8	0.1	
			Merwinite	51.1	12.4	0.1	36.4	
	148 *	1420	Liquid	36.8	15.8	13.3	34.1	0.39
			Spinel	0.6	27.9	71.1	0.4	
			Merwinite	50.7	12.7	0.1	36.5	
	149 *	1420	Liquid	36.5	16.5	13.3	33.7	0.40
			Spinel	0.1	28.5	71.3	0.1	
			Merwinite	50.8	12.6	0.1	36.5	
				Liquid + Mullite + Anorthite				
M52	151	1250	Liquid	7.4	6.0	24.4	62.2	0.39
			Mullite	0.1	0.6	70.2	29.1	
			Anorthite	17.7	0.4	33.3	48.6	
M39	152	1250	Liquid	8.2	5.1	23.0	63.7	0.36
			Mullite	0.1	0.5	70.7	28.7	
			Anorthite	17.1	0.4	31.8	50.7	
M18	153	1270	Liquid	6.9	5.4	22.8	64.9	0.37
			Mullite	0.1	0.4	70.9	28.6	
			Anorthite	17.4	0.5	32.3	49.8	
M18	154	1270	Liquid	7.7	5.2	23.8	63.3	0.38
			Mullite	0.1	0.3	71.2	28.4	
			Anorthite	17.7	0.4	32.4	49.5	
M39	155	1300	Liquid	8.0	4.7	23.2	64.1	0.36
			Mullite	0.1	0.4	71.2	28.3	
			Anorthite	18.0	0.4	33.4	48.2	
M52	156	1300	Liquid	8.0	5.6	24.2	62.2	0.39
			Mullite	0.1	0.4	71.4	28.1	
			Anorthite	18.7	0.5	34.6	46.2	
M10	157	1300	Liquid	8.7	3.0	23.4	64.9	0.36
			Mullite	0.2	0.1	72.2	27.5	
			Anorthite	17.4	0.2	31.8	50.6	
M18	158	1310	Liquid	9.1	4.2	24.8	61.9	0.40
			Mullite	0.2	0.2	71.7	27.9	
			Anorthite	18.3	0.3	33.7	47.7	

* Experimental data from previous work [15–18,23].

Table A3. Experimental Results in the System CaO-MgO-Al_2O_3-SiO_2 system with Al_2O_3/SiO_2 weight ratio of 0.4.

Mixture				Compositions (mol%)				
No.	**No.**	**T (°C)**	**Phases**	**CaO**	**MgO**	**Al_2O_3**	**SiO_2**	**Al_2O_3/SiO_2**
				Liquid only				
M20	1	1250	Liquid	30.7	17.2	10.1	42.0	0.41
M26	2	1250	Liquid	29.4	14.6	11.8	44.2	0.45
M34	3	1250	Liquid	17.9	18.4	12.2	51.5	0.40
M16	4	1280	Liquid	13.3	7.4	15.0	64.3	0.40
M16	5	1300	Liquid	13.3	7.3	15.2	64.2	0.40
M34	6	1300	Liquid	17.8	18.4	12.1	51.7	0.40
M35	7	1300	Liquid	10.9	11.1	14.5	63.5	0.39
M36	8	1300	Liquid	7.7	7.8	13.5	71.0	0.32
M42	9	1300	Liquid	24.2	19.0	11.1	45.7	0.41
M48	10	1300	Liquid	26.2	20.7	10.4	42.7	0.42
M42	11	1310	Liquid	23.6	19.7	11.0	45.7	0.41
M19	12	1320	Liquid	24.8	13.8	11.8	49.6	0.41
M42	13	1320	Liquid	25.7	20.6	10.4	43.3	0.41
M25	14	1330	Liquid	33.1	19.1	9.2	38.6	0.40
M25	15	1330	Liquid	34.3	17.7	9.4	38.6	0.41
M48	16	1340	Liquid	24.5	18.9	11.4	45.2	0.43
M13	17	1350	Liquid	33.0	28.4	7.4	31.2	0.40
M16	18	1350	Liquid	13.3	7.2	14.9	64.6	0.39
M19	19	1350	Liquid	24.2	13.4	12.0	50.4	0.40
M25	20	1350	Liquid	33.4	18.8	9.0	38.8	0.39
M51	21	1350	Liquid	20.1	10.7	14.3	54.9	0.44
M51	22	1350	Liquid	20.8	11.5	14.7	53.0	0.47
M29	23	1350	Liquid	24.1	24.3	9.8	41.8	0.40
M42	24	1350	Liquid	26.2	18.5	12.0	43.3	0.47
M44	25	1350	Liquid	27.7	23.8	9.3	39.2	0.40
M49	26	1350	Liquid	14.5	12.0	14.3	59.2	0.41
M16	27	1350	Liquid	13.2	7.4	15.1	64.3	0.40
M35	28	1350	Liquid	11.2	11.1	14.9	62.8	0.40
M22	29	1390	Liquid	37.6	20.8	8.0	33.6	0.40
M22	30	1400	Liquid	37.6	20.2	7.8	34.4	0.38
M28	31	1400	Liquid	29.8	29.6	7.8	32.8	0.41
M41	32	1400	Liquid	22.8	18.2	13.5	45.5	0.50
M49	33	1400	Liquid	16.6	13.3	15.8	54.3	0.49
M21	34	1400	Liquid	36.8	20.6	8.2	34.4	0.41
M23	35	1450	Liquid	39.7	20.3	7.2	32.8	0.37
M23	36	1450	Liquid	40.0	22.4	7.2	30.4	0.40
M47	37	1450	Liquid	34.0	26.7	7.3	32.0	0.39
M23	38	1450	Liquid	39.7	22.0	7.6	30.7	0.42
M14	39	1480	Liquid	17.9	4.8	20.0	57.3	0.59
M14	40	1500	Liquid	17.9	5.0	20.0	57.1	0.59
M23	41	1500	Liquid	40.1	22.5	7.2	30.2	0.40
M30	42	1500	Liquid	50.0	1.7	10.9	37.4	0.50
M47	43	1500	Liquid	34.1	26.9	7.5	31.5	0.40
				Liquid + Melilite				
M20	44	1230	Liquid	29.6	17.0	10.4	43.0	0.41
			melilite	41.3	17.1	3.5	38.1	
M7	45	1250	Liquid	36.0	9.5	10.6	43.9	0.41
			melilite	42.4	15.0	5.9	36.7	
M43	46	1250	Liquid	29.2	16.9	10.5	43.4	0.41
			melilite	40.6	17.4	3.2	38.8	
	47 *	1280	Liquid	33.8	14.2	9.6	42.4	0.38
			melilite	9.0	58.2	21.9	10.9	

Table A3. *Cont.*

Mixture				Compositions (mol%)				
No.	**No.**	**T (°C)**	**Phases**	**CaO**	**MgO**	**Al_2O_3**	**SiO_2**	**Al_2O_3/SiO_2**
M7	48	1300	Liquid	37.4	9.9	9.9	42.8	0.39
			melilite	43.7	12.4	7.2	36.7	
	49 *	1300	Liquid	40.4	7.2	10.0	42.4	0.40
			melilite	30.6	53.4	9.6	6.4	
M21	50	1350	Liquid	32.6	24.1	8.3	35.0	0.40
			melilite	43.0	14.1	7.6	35.3	
M17	51	1350	Liquid	9.9	5.7	14.8	69.6	0.36
			melilite	0.2	0.4	61.4	38.0	
M3	52	1350	Liquid	39.0	10.8	9.1	41.1	0.37
			melilite	43.6	12.4	9.3	34.7	
	53 *	1360	Liquid	48.0	0.0	10.0	42.0	0.40
			melilite	49.6	0.0	24.5	25.9	
M22	54	1370	Liquid	36.1	22.8	7.7	33.4	0.39
			melilite	43.5	12.8	9.4	34.3	
M21	55	1380	Liquid	36.5	20.6	8.4	34.5	0.41
			melilite	44.6	12.0	9.8	33.6	
M6	56	1400	Liquid	42.1	11.9	8.5	37.5	0.39
			melilite	46.2	8.7	13.8	31.3	
	57 *	1420	Liquid	44.9	7.7	9.1	38.3	0.40
			melilite	47.2	6.2	16.9	29.7	
	58 *	1420	Liquid	43.7	10.2	8.6	37.5	0.39
			melilite	46.0	8.0	15.0	31.0	
	59 *	1430	Liquid	52.2	0.0	9.2	38.6	0.40
			melilite	50.5	0.0	24.3	25.2	
	60 *	1450	Liquid	47.9	8.1	8.5	35.5	0.41
			melilite	47.7	4.6	19.1	28.6	
	61 *	1450	Liquid	52.9	0.0	9.0	38.1	0.40
			melilite	50.0	0.0	24.8	25.2	
	62 *	1450	Liquid	51.6	3.0	8.4	37.0	0.39
			melilite	48.9	2.3	21.9	26.9	
	63 *	1450	Liquid	53.6	0.0	8.7	37.7	0.39
			melilite	50.0	0.0	25.0	25.0	
				Liquid + Anorthite				
M26	64	1250	Liquid	29.5	16.9	10.0	43.6	0.39
			Anorthite	25.0	0.3	24.0	50.7	
M35	65	1250	Liquid	34.8	10.2	9.7	45.3	0.36
			Anorthite	24.9	0.5	24.3	50.3	
M43	66	1280	Liquid	23.4	19.8	10.7	46.1	0.39
			Anorthite	24.9	0.7	24.1	50.3	
	67 *	1280	Liquid	36.5	7.9	10.1	45.5	0.38
			Anorthite	33.3	56.2	10.3	0.2	
M34	68	1290	Liquid	18.6	18.8	12.3	50.3	0.41
			Anorthite	24.6	1.0	23.2	51.2	
M41	69	1300	Liquid	20.1	17.4	11.6	50.9	0.39
			Anorthite	24.5	1.0	23.1	51.4	
M19	70	1300	Liquid	24.1	14.7	10.3	50.9	0.35
			Anorthite	24.7	0.9	24.2	50.2	
M5	71	1300	Liquid	31.7	9.6	10.1	48.6	0.35
			Anorthite	25.3	0.5	24.4	49.8	
M8	72	1350	Liquid	28.9	8.2	11.4	51.5	0.38
			anorthite	25.1	0.5	24.1	50.3	
M9	73	1400	Liquid	14.2	4.2	15.0	66.6	0.38
			anorthite	24.5	0.3	24.7	50.5	
				Liquid + Cordierite				
M17	74	1250	Liquid	11.0	11.4	14.8	62.8	0.40
			Cordierite	21.9	0.9	21.8	55.4	

Table A3. *Cont.*

Mixture				Compositions (mol%)				
No.	**No.**	**T (°C)**	**Phases**	**CaO**	**MgO**	**Al_2O_3**	**SiO_2**	**Al_2O_3/SiO_2**
M49	75	1300	Liquid	13.1	13.3	13.4	60.2	0.38
			Cordierite	22.7	0.9	22.8	53.6	
M40	76	1300	Liquid	11.4	9.6	14.9	64.1	0.39
			Cordierite	22.4	0.5	22.6	54.5	
M10	77	1300	Liquid	11.6	3.9	15.7	68.8	0.39
			Cordierite	21.3	0.3	21.5	56.9	
				Liquid + Mullite				
M17	78	1250	Liquid	10.4	6.0	14.9	68.7	0.37
			Mullite	0.3	0.8	56.0	42.9	
M18	79	1320	Liquid	11.1	6.0	15.8	67.1	0.40
			Mullite	0.3	0.4	59.0	40.3	
M39	80	1350	Liquid	9.2	7.6	15.7	67.5	0.39
			Mullite	0.2	0.6	58.8	40.4	
M36	81	1400	Liquid	7.1	7.3	14.9	70.7	0.36
			Mullite	0.3	0.6	60.8	38.2	
M12	82	1400	Liquid	11.1	3.0	15.4	70.5	0.37
			Mullite	0.2	0.2	60.0	39.6	
M11	83	1450	Liquid	9.9	3.0	16.2	70.9	0.39
			Mullite	0.2	0.0	62.6	37.2	
M50	84	1500	Liquid	6.9	5.7	15.6	71.8	0.37
			Mullite	0.2	0.2	61.6	38.0	
				Liquid + Spinel				
M29	85	1320	Liquid	26.6	22.0	10.7	40.7	0.45
			Spinel	0.0	50.0	49.9	0.1	
M44	86	1350	Liquid	28.0	23.7	9.3	39.0	0.40
			Spinel	0.1	50.0	49.8	0.1	
M22	87	1370	Liquid	36.4	22.4	7.8	33.4	0.39
			Spinel	0.0	49.9	50.0	0.1	
	89 *	1500	liquid	30.4	30.4	7.8	31.4	0.42
			Spinel	0.5	0.8	58.7	40.0	
				Liquid + Mg_2SiO_4				
M48	90	1250	Liquid	27.6	17.4	11.0	44.0	0.42
			Mg_2SiO_4	0.8	66.5	0.0	32.7	
M38	91	1250	Liquid	29.3	17.4	10.1	43.2	0.40
			Mg_2SiO_4	1.3	65.5	0.0	33.2	
M44	92	1250	Liquid	28.8	17.7	10.7	42.8	0.42
			Mg_2SiO_4	1.2	66.0	0.2	32.6	
M32	93	1300	Liquid	21.7	21.4	10.8	46.1	0.40
			Mg_2SiO_4	0.5	66.3	0.0	33.2	
M29	94	1300	Liquid	26.1	20.6	10.6	42.7	0.42
			Mg_2SiO_4	0.9	66.1	0.1	32.9	
M38	95	1300	Liquid	27.3	20.8	10.0	41.9	0.41
			Mg_2SiO_4	1.1	65.6	0.1	33.2	
M28	96	1300	Liquid	41.6	16.5	4.4	37.5	0.20
			Mg_2SiO_4	3.5	63.5	0.1	32.9	
M29	97	1330	Liquid	25.4	22.5	10.3	41.8	0.42
			Mg_2SiO_4	0.9	66.2	0.1	32.8	
M31	98	1350	Liquid	29.9	23.8	7.9	38.4	0.35
			Mg_2SiO_4	2.0	65.0	0.2	32.8	
M31	99	1400	Liquid	28.1	26.3	7.6	38.0	0.34
			Mg_2SiO_4	2.2	64.8	0.1	32.9	
M44	100	1400	Liquid	29.2	21.5	9.1	40.2	0.38
			Mg_2SiO_4	0.5	66.3	0.0	33.2	
				Liquid + MgO				
M30	101	1450	Liquid	33.7	27.2	7.5	31.6	0.40
			MgO	0.1	99.5	0.4	0.0	

Table A3. *Cont.*

Mixture				Compositions (mol%)				
No.	**No.**	**T (°C)**	**Phases**	**CaO**	**MgO**	**Al_2O_3**	**SiO_2**	**Al_2O_3/SiO_2**
M23	102	1470	Liquid	40.1	22.1	7.2	30.6	0.40
			MgO	0.2	99.5	0.3	0.0	
	103 *	1500	Liquid	29.8	31.6	7.4	31.2	0.40
			MgO	0.1	0.3	0.7	98.9	
	104 *	1500	Liquid	42.2	20.8	6.9	30.1	0.39
			MgO	0.2	99.5	0.3	0.0	
M27	105	1500	Liquid	39.3	23.1	7.0	30.6	0.39
			MgO	0.1	99.6	0.3	0.0	
M30	106	1500	Liquid	33.0	28.5	7.4	31.1	0.40
			MgO	0.1	99.5	0.4	0.0	
M30	107	1500	Liquid	33.0	28.4	7.4	31.2	0.40
			MgO	0.1	99.5	0.4	0.0	
M30	108	1500	Liquid	33.0	28.5	7.4	31.1	0.40
			MgO	0.1	99.5	0.4	0.0	
M37	109	1500	Liquid	37.0	24.9	7.3	30.8	0.40
			MgO	0.2	99.4	0.4	0.0	
M27	110	1550	Liquid	38.5	24.2	7.1	30.2	0.40
			MgO	0.1	99.5	0.4	0.0	
M24	111	1550	Liquid	46.0	18.6	6.8	28.6	0.40
			MgO	0.2	99.6	0.2	0.0	
M46	112	1550	Liquid	41.9	21.1	7.1	29.9	0.40
			MgO	0.2	99.5	0.3	0.0	
M46	113	1550	Liquid	41.2	22.4	7.2	29.2	0.42
			MgO	0.2	99.5	0.3	0.0	
M37	114	1550	Liquid	36.8	25.9	7.1	30.2	0.40
			MgO	0.1	99.5	0.4	0.0	
				Liquid + Merwinite				
	115*	1400	Liquid	38.9	20.4	7.4	33.3	0.38
			Merwinite	49.8	17.2	0.1	32.9	
M2	116	1400	Liquid	43.5	13.2	8.5	34.8	0.42
			Merwinite	49.8	16.7	0.1	33.4	
M23	117	1430	Liquid	40.5	22.4	7.5	29.6	0.43
			Merwinite	50.9	17.7	0.1	31.3	
	118 *	1450	Liquid	45.2	14.1	8.0	32.7	0.41
			Merwinite	50.0	16.6	0.1	33.3	
M23	119	1450	Liquid	40.9	21.6	7.3	30.2	0.41
			Merwinite	50.3	17.4	0.1	32.2	
				Liquid + Ca_2SiO_4				
M4	120	1500	Liquid	47.2	13.4	7.7	31.7	0.41
			Ca_2SiO_4	62.4	4.1	0.1	33.4	
				Liquid + Melilite + Spinel				
M25	121	1300	Liquid	30.6	20.3	9.3	39.8	0.40
			Melilite	42.4	14.6	6.6	36.4	
			Spinel	0.1	49.9	49.9	0.1	
M25	122	1320	Liquid	32.8	18.1	9.7	39.4	0.42
			Melilite	42.8	14.6	6.8	35.8	
			Spinel	0.1	50.3	49.5	0.1	
				Liquid + Melilite + Anorthite				
M15	123	1250	Liquid	32.7	14.0	10.4	42.9	0.41
			Anorthite	25.4	0.7	24.9	49.0	
			Melilite	42.1	15.8	5.4	36.7	
M1	124	1250	Liquid	34.8	10.3	9.8	45.1	0.37
			Anorthite	25.3	0.2	24.4	50.1	
			Melilite	41.5	16.2	4.1	38.2	

Table A3. *Cont.*

Mixture				Compositions (mol%)				
No.	**No.**	**T (°C)**	**Phases**	**CaO**	**MgO**	**Al_2O_3**	**SiO_2**	**Al_2O_3/SiO_2**
				Liquid + Melilite + Mg_2SiO_4				
M20	125	1220	Liquid	29.1	16.6	11.1	43.2	0.44
			Mg_2SiO_4	1.1	66.2	0.1	32.6	
			Melilite	41.3	16.6	3.9	38.2	
M25	126	1250	Liquid	28.8	19.2	10.4	41.6	0.43
			Mg_2SiO_4	1.3	65.9	0.1	32.7	
			Melilite	42.0	14.3	7.0	36.7	
M45	127	1300	Liquid	30.3	20.2	8.9	40.6	0.37
			Mg_2SiO_4	2.0	64.9	0.2	32.9	
			Melilite	42.3	14.5	6.9	36.3	
M44	128	1300	Liquid	26.2	20.6	7.2	46.0	0.56
			Mg_2SiO_4	41.5	15.8	4.8	37.9	
			Melilite	1.8	64.8	0.8	32.6	
M28	129	1350	Liquid	31.5	23.4	7.2	37.9	
			Mg_2SiO_4	41.3	16.8	3.8	38.1	
			Melilite	3.3	63.6	0.1	33.0	
M45	130	1350	Liquid	30.8	23.5	7.6	38.1	0.34
			Mg_2SiO_4	3.5	63.7	0.1	32.7	
			Melilite	40.7	17.7	3.9	37.7	
M45	131	1450	Liquid	34.4	22.5	5.8	37.3	0.34
			Mg_2SiO_4	3.5	63.3	0.2	33.0	
			Melilite	41.8	16.6	4.4	37.2	
				Liquid + Mg_2SiO_4 + Anorthite				
M42	132	1200	Liquid	24.0	22.2	7.9	45.9	0.29
			Anorthite	24.1	1.4	23.3	51.2	
			Mg_2SiO_4	1.0	66.1	0.1	32.8	
M42	133	1230	Liquid	24.1	19.9	10.2	45.8	0.38
			Anorthite	24.9	0.9	24.2	50.0	
			Mg_2SiO_4	0.7	66.5	0.0	32.8	
M20	134	1230	Liquid	27.5	17.8	10.0	44.7	0.38
			Anorthite	24.8	0.3	24.1	50.8	
			Mg_2SiO_4	0.8	65.9	0.1	33.2	
M34	135	1240	Liquid	17.2	18.0	9.1	55.7	0.28
			Anorthite	24.1	1.7	22.1	52.1	
			Mg_2SiO_4	0.2	66.9	0.0	32.9	
M34	136	1250	Liquid	18.4	19.3	9.2	53.1	0.29
			Anorthite	24.1	1.5	22.6	51.8	
			Mg_2SiO_4	0.2	66.7	0.0	33.1	
M41	137	1250	Liquid	17.5	19.3	9.2	54.0	0.29
			Anorthite	24.0	1.5	22.9	51.6	
			Mg_2SiO_4	0.4	66.9	0.0	32.7	
M42	138	1250	Liquid	28.6	17.6	10.2	43.6	0.40
			Anorthite	24.9	0.9	23.5	50.7	
			Mg_2SiO_4	0.7	66.2	0.1	33.0	
				Liquid + Mg_2SiO_4 + Spinel				
M28	139	1400	Liquid	31.4	27.9	6.2	34.5	0.30
			Spinel	0.0	49.8	49.7	0.5	
			Mg_2SiO_4	3.7	63.2	0.1	33.0	
M28	140	1400	Liquid	30.7	27.6	6.3	35.4	0.30
			Spinel	0.0	50.4	49.4	0.2	
			Mg_2SiO_4	4.0	63.2	0.1	32.7	
M28	141	1400	Liquid	30.8	27.6	6.5	35.1	0.31
			Spinel	0.0	49.8	49.7	0.5	
			Mg_2SiO_4	3.7	63.2	0.1	33.0	

Table A3. *Cont.*

Mixture				Compositions (mol%)				
No.	**No.**	**T (°C)**	**Phases**	**CaO**	**MgO**	**Al_2O_3**	**SiO_2**	**Al_2O_3/SiO_2**
				Liquid + Merwinite + MgO				
M23	142	1450	Liquid	39.7	22.0	7.6	30.7	0.42
			MgO	0.2	99.5	0.3	0.0	
			Merwinite	49.5	17.2	0.1	33.2	
				Liquid + MgO + Ca_2SiO_4				
M24	143	1550	Liquid	45.6	19.0	6.7	28.7	0.40
			Ca_2SiO_4	61.5	5.2	0.1	33.2	
			MgO	0.2	99.5	0.3	0.0	
M24	144	1550	Liquid	44.3	18.8	9.8	27.1	0.30
			Ca_2SiO_4	50.3	16.7	0.1	32.9	
			MgO	0.2	99.5	0.3	0.0	
				Liquid + MgO + Spinel				
M47	145	1430	Liquid	35.0	26.1	6.9	32.0	0.37
			Spinel	0.3	49.8	49.8	0.1	
			MgO	0.1	99.6	0.3	0.0	
M33	146	1450	Liquid	30.3	30.2	6.9	32.6	0.36
			Spinel	0.0	50.3	49.5	0.2	
			MgO	0.1	99.5	0.4	0.0	
				Liquid + Merwinite + Spinel				
	147 *	1400	Liquid	38.7	20.5	7.9	32.9	0.41
			Spinel	0.1	49.8	50.0	0.1	
			Merwinite	49.8	17.0	0.1	33.1	
	148 *	1420	Liquid	37.5	22.6	7.5	32.4	0.39
			Spinel	0.8	49.3	49.4	0.5	
			Merwinite	49.4	17.3	0.1	33.2	
	149 *	1420	Liquid	37.2	23.5	7.4	31.9	0.40
			Spinel	0.1	50.4	49.4	0.1	
			Merwinite	49.5	17.2	0.1	33.2	
				Liquid + Mullite + Anorthite				
M52	151	1250	Liquid	8.5	9.6	15.4	66.5	0.39
			Mullite	0.1	1.3	57.9	40.7	
			Anorthite	21.6	0.7	22.4	55.3	
M39	152	1250	Liquid	9.4	8.2	14.5	67.9	0.36
			Mullite	0.2	1.1	58.4	40.3	
			Anorthite	20.8	0.7	21.2	57.3	
M18	153	1270	Liquid	7.9	8.6	14.3	69.2	0.37
			Mullite	0.2	0.8	58.8	40.2	
			Anorthite	21.1	0.9	21.6	56.4	
M18	154	1270	Liquid	8.8	8.4	15.0	67.8	0.38
			Mullite	0.2	0.6	59.2	40.0	
			Anorthite	21.5	0.7	21.7	56.1	
M39	155	1300	Liquid	9.2	7.6	14.7	68.5	0.36
			Mullite	0.2	0.8	59.1	39.9	
			Anorthite	22.0	0.7	22.4	54.9	
M52	156	1300	Liquid	9.2	9.0	15.3	66.5	0.39
			Mullite	0.2	0.8	59.4	39.6	
			Anorthite	22.9	0.9	23.3	52.9	
M10	157	1300	Liquid	10.1	4.9	14.9	70.1	0.36
			Mullite	0.3	0.2	60.4	39.1	
			Anorthite	21.1	0.3	21.2	57.4	
M18	158	1310	Liquid	10.5	6.8	15.8	66.9	0.40
			Mullite	0.3	0.4	59.8	39.5	
			Anorthite	22.4	0.5	22.7	54.4	

* Experimental data from previous work [15–18,23].

References

1. Geerdes, M.; Chaigneau, R.; Lingiardi, O.; Molenaar, R.; van Opbergen, R.; Sha, Y.; Warren, P. Chapter XI—Operation Challenges. In *Modern Blast Furnace Ironmaking: An Introduction*, 4th ed.; Ios Press: Amsterdam, The Netherlands, 2020; pp. 197–226, ISBN 978-1-64368-122-8.
2. Sunahara, K.; Nakano, K.; Hoshi, M.; Inada, T.; Komatsu, S.; Yamamoto, T. Effect of high Al_2O_3 slag on the blast furnace operations. *ISIJ Int.* **2008**, *48*, 420–429. [CrossRef]
3. Yi, Z.; Liu, Q.; Shao, H. Effect of MgO on highly basic sinters with high Al_2O_3. *Min. Metall. Explor.* **2021**, *38*, 2175–2183. [CrossRef]
4. Talapaneni, T.; Yedla, N.; Sarkar, S.; Pal, S. Effect of basicity, Al_2O_3 and MgO content on the softening and melting properties of the CaO-MgO-SiO_2-Al_2O_3 high alumina quaternary slag system. *Metall. Res. Technol.* **2016**, *113*, 501.
5. Hu, X.; Lin, L.; Li, L. Laboratory research on property of higher Al_2O_3 content slag. *China Metall.* **2006**, *16*, 36–41. (In Chinese)
6. Wang, P.; Meng, Q.; Long, H.; Li, J. Influence of basicity and MgO on fluidity and desulfurization ability of high aluminum slag. *High Tem. Mat. Process.* **2016**, *35*, 669–675. [CrossRef]
7. Bai, K.; Zuo, H.; Liu, W.; Wang, J.; Chen, J.; Xue, Q. Effect of quaternary basicity on softening–melting behavior of primary slag based on magnesium flux pellet. *J. Iron Steel Res. Int.* **2022**, *29*, 1185–1193. [CrossRef]
8. Prince, A.T. Phase Equilibrium relationships in a portion of the system MgO-Al_2O_3-2CaO·SiO_2. *J. Am. Ceram. Soc.* **1951**, *34*, 44–51. [CrossRef]
9. DeVries, R.C.; Osborn, E.F. Phase equilibria in High-alumina part of the system CaO-MgO-Al_2O_3-SiO_2. *J. Am. Ceram. Soc.* **1957**, *40*, 6–15. [CrossRef]
10. DeVries, R.C.; Osborn, E.F.; Gee, K.H.; Kraner, H.M. Optimum composition of blast furnace slag as deduced for the quaternary system CaO-MgO-Al_2O_3-SiO_2. *Trans. AIME* **1954**, *6*, 33–45.
11. Prince, A.T. Liquidus relationships on 10% MgO plane of the system lime-magnesia-alumina-silica. *J. Am. Ceram. Soc.* **1954**, *37*, 402–408. [CrossRef]
12. Cavalier, G.; Sandrea-Deudon, M. Quaternary slags CaO-MgO-Al_2O_3-SiO_2: Liquidus surfaces and crystallisation paths for constant magnesia concentrations. *Rev. Metall.* **1960**, *5*, 1143–1157. [CrossRef]
13. Gutt, W.; Russel, A.D. Studies of the system CaO-SiO_2-Al_2O_3-MgO in relation to the stability of blast furnace slag. *J. Mater. Sci.* **1977**, *12*, 1869–1878. [CrossRef]
14. Dahl, F.; Brandberg, J.; Du, S. Characterization of melting of some slags in the Al_2O_3-CaO-MgO-SiO_2 quaternary system. *ISIJ Int.* **2006**, *46*, 614–616.
15. Ma, X.; Wang, G.; Wu, S.; Zhu, J.; Zhao, B. Phase equilibria in the CaO-SiO_2-Al_2O_3-MgO System with CaO/SiO_2 ratio of 1.3 relevant to iron blast furnace slags. *ISIJ Int.* **2015**, *55*, 2310–2317.
16. Ma, X.; Zhang, D.; Zhao, Z.; Evans, T.; Zhao, B. Phase equilibria studies in the CaO-SiO_2-Al_2O_3-MgO system with CaO/SiO_2 ratio of 1.10. *ISIJ Int.* **2016**, *56*, 513–519. [CrossRef]
17. Kou, M.; Wu, S.; Ma, X.; Wang, L.; Chen, M.; Cai, Q.; Zhao, B. Phase equilibrium studies of CaO-SiO_2-Al_2O_3-MgO system with binary basicity of 1.5 related to blast furnace slag. *Metall. Mater. Trans. B* **2016**, *47*, 1093–1102. [CrossRef]
18. Wang, D.; Chen, M.; Jiang, Y.; Wang, S.; Zhao, Z.; Evans, T.; Zhao, B. Phase equilibria studies in the CaO-SiO_2-Al_2O_3-MgO system with CaO/SiO_2 ratio of 0.9. *J. Am. Ceram. Soc.* **2020**, *103*, 7299–7309.
19. Gran, J.; Wang, Y.; Du, S. Experimental determination of the liquidus in the high basicity region in the Al_2O_3 (30 mass%)-CaO-MgO-SiO_2 system. *Calphad* **2011**, *35*, 249–254. [CrossRef]
20. Gran, J.; Yan, B.; Du, S. Experimental determination of the liquidus in the high-basicity region in the Al_2O_3 (25 mass pct)-CaO-MgO-SiO_2 and Al_2O_3 (35 mass pct)-CaO-MgO-SiO_2 systems. *Metall. Mater. Trans. B* **2011**, *42*, 1008–1016. [CrossRef]
21. Lyu, S.; Ma, X.; Chen, M.; Huang, Z.; Wang, G. Application of phase equilibrium studies of CaO–SiO_2–Al_2O_3–MgO system for oxide inclusions in Si-deoxidized steels. *Calphad* **2020**, *68*, 101721. [CrossRef]
22. Lyu, S.; Ma, X.; Huang, Z.; Yao, Z.; Lee, H.; Jiang, Z.; Wang, G.; Zou, J.; Zhao, B. Inclusion characterization and formation mechanisms in spring steel deoxidized by silicon. *Metall. Mater. Trans. B* **2019**, *5*, 732–747. [CrossRef]
23. Yao, Z.; Ma, X.; Lyu, S. Phase equilibria of the Al_2O_3–CaO–SiO_2-(0%, 5%, 10%) MgO slag system for non-metallic inclusions control. *Calphad* **2021**, *72*, 102227. [CrossRef]
24. *Verein Duetscher Eisenhuttenleute: Slag Atlas*; Verlag Sthaleisen GmbH: Düsseldorf, Germany, 1995; p. 156.
25. Bale, C.W.; Bélisle, E.; Chartrand, P.; Decterov, S.; Eriksson, G.; Gheribi, A.; Hack, K.; Jung, I.H.; Kang, Y.B.; Melançon, J.; et al. Reprint of: FactSage thermochemical software and databases, 2010–2016. *Calphad* **2016**, *55*, 1–19. [CrossRef]
26. Sundman, B.; Jansson, B.; Andersson, J.O. The thermo-calc databank system. *Calphad* **1985**, *9*, 153–190.
27. Xu, R.Z.; Zhang, H.S.; Zhang, J.L.; Liu, C.J.; Wang, Z.Y. Evaluation of Jingtang blast furnace slag properties and analysis of low MgO slag performance. *Chin. Metall.* **2016**, *26*, 16–20. (In Chinese)
28. Muan, A.; Osborn, E.F. *Phase Equilibria Among Oxides in Steelmaking*; Addison-Wesley Publishing Company: Boston, MA, USA, 1965; pp. 148–157.

Disclaimer/Publisher's Note: The statements, opinions and data contained in all publications are solely those of the individual author(s) and contributor(s) and not of MDPI and/or the editor(s). MDPI and/or the editor(s) disclaim responsibility for any injury to people or property resulting from any ideas, methods, instructions or products referred to in the content.